STRUCTURAL AND HYDROLOGICAL INFLUENCES ON THE EVOLUTION OF HELLHOLE CAVE, PENDLETON COUNTY, WEST VIRGINIA

A Thesis

Presented to

The Graduate Faculty of the University of Akron

In Partial Fulfillment

of the Requirements for the Degree

Master of Science

Daniel Zinz

May, 2007

STRUCTURAL AND HYDROLOGICAL INFLUENCES ON THE EVOLUTION OF HELLHOLE CAVE, PENDLETON COUNTY, WEST VIRGINIA

Daniel Zinz

Thesis

Approved:	Accepted:
_____	_____
Advisor Dr. Ira D. Sasowsky	Dean of the College Dr. Ronald F. Levant
_____	_____
Committee Member Dr. David McConnell	Dean of the Graduate School Dr. George R. Newkome
_____	_____
Committee Member Dr. John Peck	Date
_____	
Department Chair Dr. John Szabo	

ABSTRACT

Hellhole is an extensive (32 kilometer) cave system developed within Germany Valley (Pendleton County, West Virginia) on the flank of the Wills Mountain Anticline. The area can be described as a mature karst aquifer on the transitional margin of the Appalachian Plateau and Valley and Ridge physiographic provinces. Hellhole is the most extensive and deepest (158 meters) of several mapped caves in the area (others include Memorial Day Cave and Schoolhouse Cave). The upper bounding lithology is the McGlone Limestone. The cave penetrates through the Big Valley Formation and in to the New Market Limestone, a high purity unit that is mined locally. Faulting and folding are prominently exposed in several passages, but did not affect passage development in a noticeable way. The entrance sinkhole opens in to a large room, however, the morphology of the room suggests that the room formed the entrance by the intersection of passages followed by a vertical shaft intersecting from the surface. Passage orientation and strike of the bedrock are nearly identical (N25°E). Lower passages are generally down dip from upper (older) passages. Cave sediment and paleomagnetic analysis reveals that the minimum age of sediments analyzed are 1.070 million years old. Three hundred measurements of wall scallops show that paleowaters in the Western section flowed southwest (1.1 cubic meters per second). Paleoflow from the Southern portion of the cave flowed northward (0.94 meters cubic meters per second),

and flow in the Northern section flowed southward (1.0 cubic meters per second). Most passages are 50 to 100 meters below the present land surface. Most of the cave appears to have formed under phreatic conditions, but the presence of thick clastic sediments in some locations attests to vadose invasion.

ACKNOWLEDGEMENTS

There are many individuals that aided me in this project. The individual that I owe the greatest gratitude to is my thesis advisor, Dr. Ira Sasowsky. He has helped me throughout this project in the office, in the field, and by motivating me at home.

I also would like to acknowledge members of my thesis committee, Dr. Dave McConnell and Dr. John Peck. I want to thank them for their comments and revisions on the reporting of this investigation. Dr. McConnell's experience in the area of this project was very helpful. I appreciate Dr. Peck's flexibility, as he joined my committee late in this project when I needed him most.

Many thanks go to Gordon Brace and the Germany Valley Karst Survey, who knew nothing of my personality or abilities but still warmly invited me in to the GVKS. Two individuals that have guided me through Hellhole, mentoring me along the way are Miles Drake and Lewis Carroll. Without the help and support of the GVKS, Gordon Brace, Miles Drake, and Lewis Carroll this investigation never would have begun.

Some of the other individuals that I owe gratitude toward for their role in this study are: Larry Kisamore, local resident, has allowed me to stay at a house, on his farm and supported my investigation and the cave survey effort of the GVKS. Joe Dean, Greer Limestone Quarry Manager, granted the GVKS; permission to diagnose and survey the cave; Bill Harbert of the University of Pittsburgh (paleomagnetism lab), allowed me to

analyze my sediment samples in his lab using his equipment; Rebecca Bixby, friend and fellow caver, helped me with the mobilization, collection, and removal of my paleomagnetic sediment samples in Hellhole.

Finally, without the support of my lovely wife, Bessie, the trips to West Virginia, the research, and the long nights of typing would not have ever have been permitted. To her, I owe a big thank you. I hope she has continued support of further investigation.

TABLE OF CONTENTS

LIST OF TABLES ix
LIST OF FIGURES x
CHAPTER
I. INTRODUCTION 1
II. BACKGROUND 6
III. INVESTIGATION OF STRUCTURAL GEOLOGY 17
Introduction 17
Methods 18
Results 20
IV. CAVE SEDIMENT AND PALEOMAGNETIC INVESTIGATION 26
Introduction 26
Methods 28
Results 31
V. PALEOHYDROLOGICAL INVESTIGATION 41
Introduction 41
Methods 42
Results 43
VI. DISCUSSION AND CONCLUSIONS 49
Discussion 49
Conclusions 59
REFERENCES 61
APPENDIX A WEST VIRGINIA STATE DEPARTMENT OF HEALTH WELL COMPLETION REPORT 65

APPENDIX B STRIKE AND DIP OF BEDDING PLANES AND FAULTS FROM WITHIN AND OVER HELLHOLE 66
APPENDIX C PALEOMAGNETIC SAMPLE ORIENTATION DATA 68
APPENDIX D ZIJDERVELD DIAGRAMS 70
APPENDIX E MAGNETIC SUSCEPTIBILITY OF PALEOMAGNETIC SAMPLES. 80
APPENDIX F PALEOFLOW MEASUREMENTS AND CALCULATIONS 81

LIST OF TABLES

Table Page

1. Susceptibility results of paleomagnetic samples.....36

2. Interpretation of paleomagnetic sampling results.....37

3. Explanation of variables from Curl's flow velocity equation.....44

LIST OF FIGURES

Figure Page

1. Diagram of different cave patterns 2
2. Schematic diagram of water flow across strike and down dip 4
3. Map showing Pendleton County with respect to West Virginia political boundaries and physiographic provinces. 7
4. Major stratigraphic units of Pendleton County 8
5. Generalized cross sections of Germany Valley and surrounding area 9
6. Geologic map of Germany Valley 10
7. Geology and hydrography of Pendleton County 12
8. Color orthophotograph of the enclosed Germany Valley drainage basin 13
9. Color orthophotograph of the Germany Valley area with maps of major caves shown in red 15
10. Color orthophotograph of vicinity and map of Hellhole 16
11. Terrain visualization with major structural features in the study area 19
12. Rose diagrams of strike in Germany Valley 21
13. Rose diagram of Hellhole cave passage direction 22
14. Map of the locations of faults and strike and dip measurements 24
15. Photograph of a fault related fold in Bob's Big Break Borehole 25
16. Photograph of a fault related fold near Raccoon Passage 25
17. Map of a portion of Hellhole showing paleomagnetic sampling location 29
18. Schematic cross section of paleomagnetic sampling location 32
19. Photographic overview of inclined beds of the Sand Hill 33

20. Photograph of the Sand Hill deposit....33

21. Schmidt equal area pole plots of characteristic remnant directions from paleomagnetic samples....38

22. Stratigraphic column of Sand Hill showing paleomagnetic sediment sequence compared to geomagnetic polarity timescale....40

23. Map of paleoflow directions indicated by scallops in Hellhole....45

24. Photograph of a side passage of the Southwest Extension with scallops indicating flow out the page....48

25. Photograph showing wall and ceiling scallops in a side passage of the Southwest Extension indicating flow into the page....48

26. Schematic diagram of the entrance sink to Hellhole. Geology based upon visual observations....50

27. Entrance to Hellhole....52

28. Comparison of Hellhole, cave passage rose diagram, and the Wills Mountain anticline....54

29. Schematic diagram of the origin of the Sand Hill region of Hellhole....56

30. Schematic diagram of relationship of upper and lower aquifers present in Germany Valley....58

CHAPTER I

INTRODUCTION

Limestone caves are found in karst terrains worldwide. They form from the dissolution of limestones. Water mixes with carbon dioxide in the atmosphere and soil, forming a weak acid. The acid dissolves the limestone slowly along the route of water travel. Ground water will travel along the path of least resistance in a direction of decreasing head. This route will pass through the joints and along the bedding planes of the bedrock, and the subsequent dissolution creates voids in the rock. As time progresses, the openings may become large enough to be considered a cave, defined as natural opening large enough for a human to traverse and leading to total darkness. White (1988) and Ford and Williams (1989) provide overview of the forms and processes of karst hydrology.

There are five major patterns of caves (Palmer, 1991). These are branchwork, network, anastomotic, ramiform and spongework (Figure 1). Branchwork caves are the most common type. They are composed of radiating passages that all connect downstream to a single main conduit. Branchwork caves are the subsurface hydrologic equivalent of dendritic river channels (Palmer, 1991). Network caves form a grid-like pattern. The passages intersect at near right angles. They are the result of the widening of the fractures in soluble bedrock. Anastomotic caves consist of curvilinear tubes that

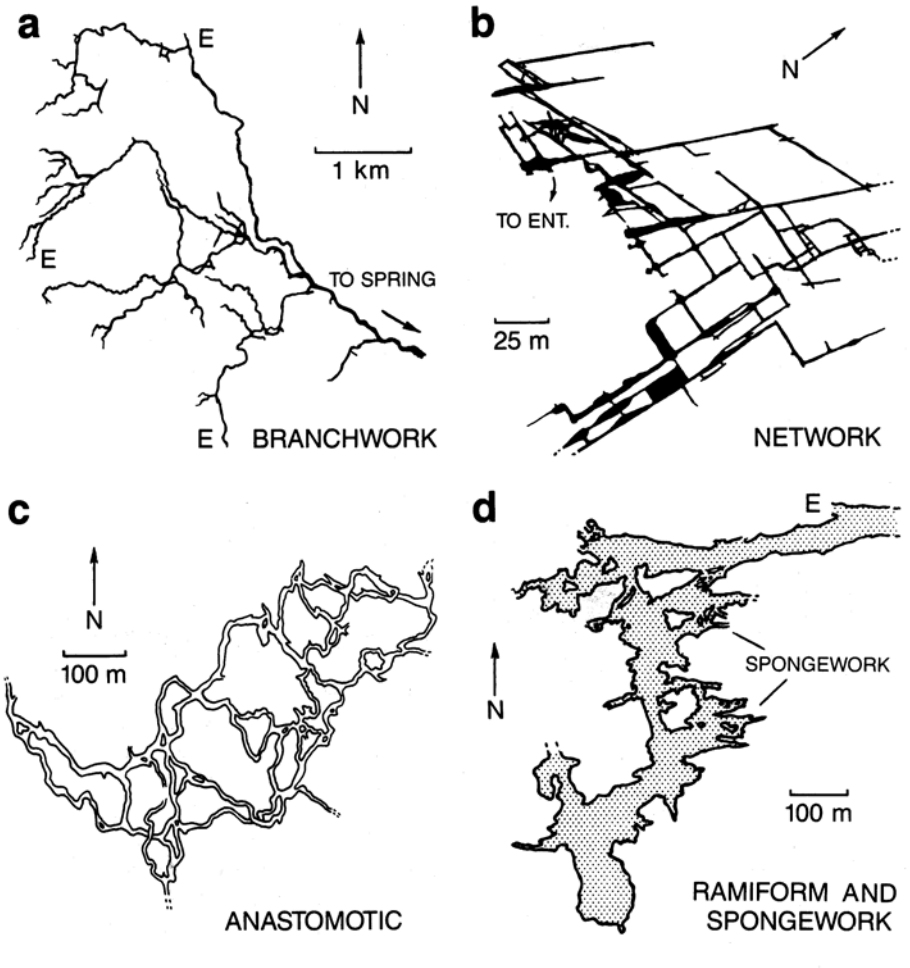

Figure 1. Diagram of different cave patterns (Palmer, 1991).

intersect in a braided pattern with many closed loops (Palmer, 1991). They form from water randomly flowing across a low angle fracture. Ramiform and spongework caves form large interconnected cavities. Spongework caves form by the coalescing of pores and minor interstices. Ramiform caves may have served as sequential outlets of water (Palmer, 1991).

Karst in the Appalachian Mountains is generally controlled by the presence of limestone within the folded valleys. The mountains are capped with resistant sandstone. The surface streams in the sandstone channel recharge waters in to the valleys. Most of the exploited valleys contain Mississippian and Ordovician age limestones. Caves develop in the subsurface as a result of surface water from streams and other sources sinking in to the valley bedrock. Limestone caves are best developed along ground-water paths of the greatest discharge and solutional aggressiveness. An understanding of cave development is essential to the hydrologic or geomorphic interpretation of any karst region (Palmer, 1991)

Cave passages (Figure 2) can develop across dip, or near parallel to bedrock strike (Davies, 1960). Valleys controlled by thrust faults, zones of fracture concentration, joints, and changes in rock type may provide ground water drains parallel to bedrock strike (Parizek, et al. 1971). According to Deike (1969), cave passages that develop in valleys parallel to an anticline axis usually develop along the bedrock strike of the valley. She states that the highest percentage of passages are within ten degrees of the strike, and that the primary joint direction follows the strike of the valley. The next highest percentage follows a secondary joint orientation near ninety degrees from the primary

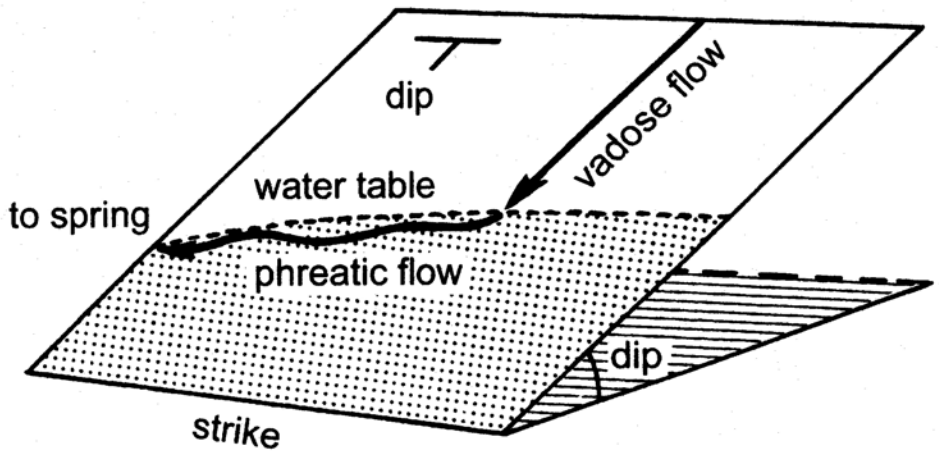

Figure 2. Schematic diagram of water flow across strike and down dip (Palmer, 1975).

joint direction. Cave passages generally cross faults without becoming enlarged.

The purpose of this study is to determine structural and hydrologic influences on the development of a mature karst aquifer underlying Germany Valley, Pendleton County, West Virginia. The site is located below a valley formed in a doubly plunging anticline, with an abundance of vertical pits and caves. The caves in this region are the focus of an intense exploration and mapping effort by the Germany Valley Karst Survey (GVKS). The primary cave for this study is Hellhole. This analysis makes use of aspects of hydrology, paleohydrology, structural geology, and paleomagnetism.

Three hypotheses are proposed for this study: 1) The major conduit of Hellhole was formed as a result of mountain surface drainage sinking, and then flowing parallel to bedrock strike, 2) The entrance sinkhole resulted from the confluence of several underground streams, and 3) Horizontal passage development in Hellhole is a result of water flowing along strike to the discharge area of Judy Springs.

CHAPTER II

BACKGROUND

Hellhole is located in Pendleton County West Virginia near the transitional margin of the Appalachian Plateau and the Valley and Ridge geomorphic province (Figure 3). The cave is in Germany Valley, which is karstified and contains virtually no surface drainage (Dasher, 2001; Sites, 1971). Germany Valley is on the axis of the Wills Mountain Anticline, a doubly plunging asymmetric fold. This anticline dominates the geology of Pendleton County and the western part of West Virginia's panhandle (Dasher, 2001). The Wills Mountain Anticline extends south from the North Fork Mountain Gap in Grant County for approximately 100 kilometers (km) into Highland County, Virginia. The core of the valley is composed of Ordovician limestones (Figure 4 through 6), one of which is the New Market limestone, sought and quarried for its purity. According to Dasher (2001), surrounding Germany Valley is an elongated "ring" of Silurian Tuscarora Sandstone. On the eastern side of this ring, the eastward-dipping Tuscarora Sandstone outcrop forms sheer and spectacular cliffs along the crest of North Fork Mountain. On the west side, where the bedding is nearly vertical, the Tuscarora Sandstone forms a series of resistant knobs, such as Wildcat Rocks, River Knobs, Nelson Rocks, Seneca Rocks, and Champe Rocks (Dasher, 2001).

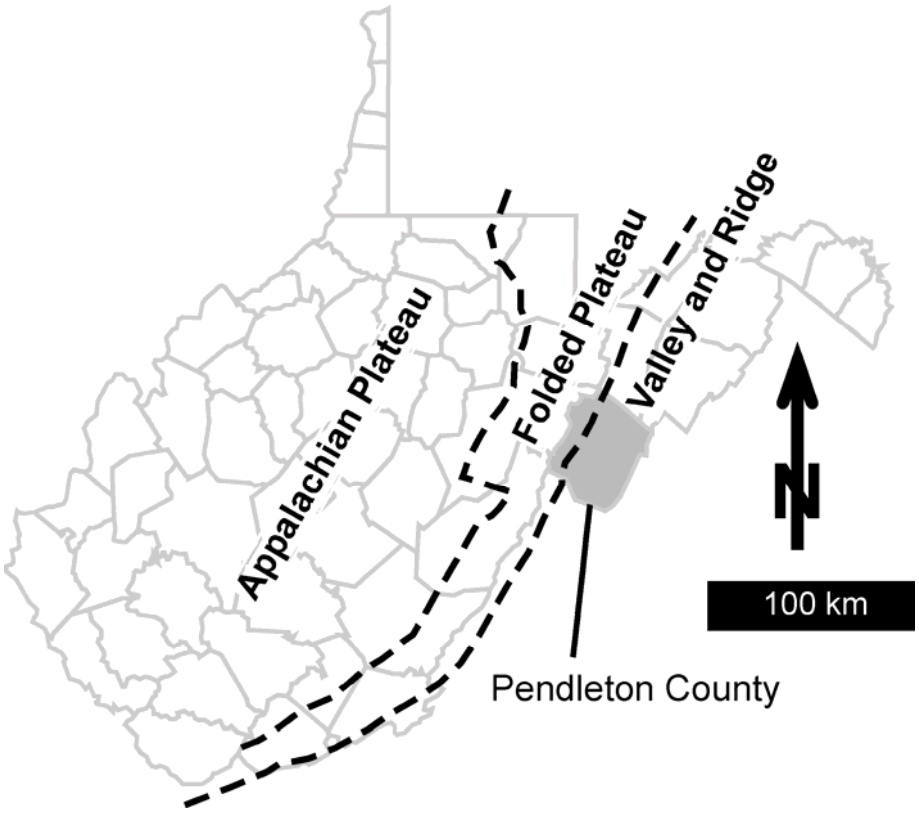

Figure 3. Map showing Pendleton County with respect to West Virginia political boundaries and physiographic provinces (after Kulander and Dean, 1986).

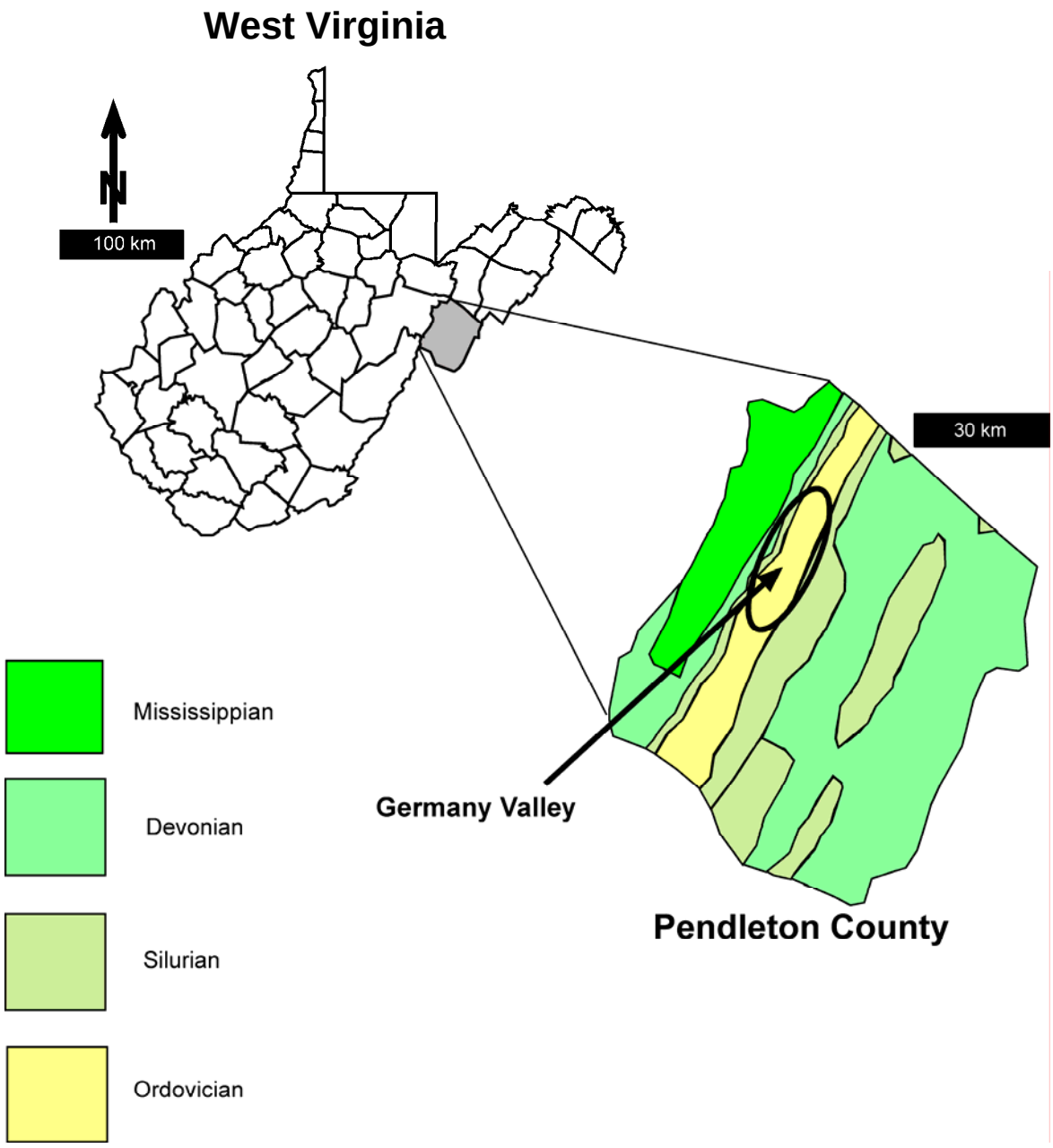

Figure 4. Major stratigraphic units of Pendleton County (after Jones, 1997).

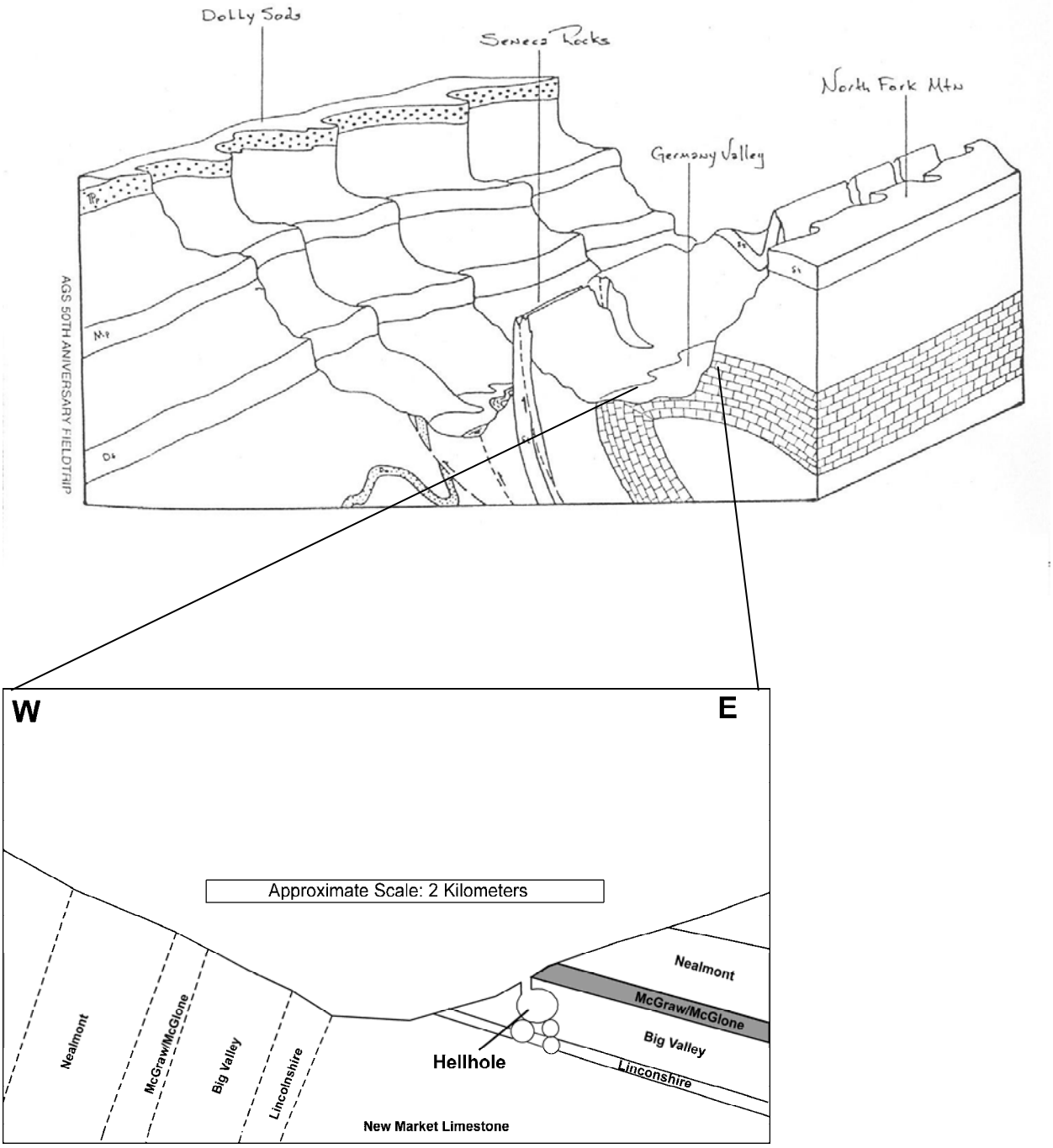

Figure 5. Generalized cross sections of Germany Valley and surrounding area. Top diagram from Drabbish and Sites (1982)

GEOLOGY OF GERMANY VALLEY
PENDLETON COUNTY, WEST VIRGINIA

Tuscarora Sandstone
A medium to thick-bedded, white to gray or pinkish sandstone; fine to coarse quartzite; primarily silica cemented. Between 150 and 250 feet thick; highly resistant and forms prominent ridges.

Juniata Formation
A thin to thick-bedded, red, cross-bedded, non-marine sandstone and siltstone; contains some shale, sandstone, and conglomerate layers. Between 200 and 300 feet thick.

Oswego Formation
A gray to light-green sandstone; cross-bedded with some pebble conglomerate layers. Between 50 and 100 feet thick.

Martinsburg Shale
A dark marine shale; contains some siltstone layers; weathers to light yellow, tan and red. Between 1500 and 2000 feet thick.

Trenton Group

Dolly Ridge Formation:
405 feet thick: Upper 307 feet interbedded argillaceous limestone, dark gray shale, and K-bentonite. Lower 98 feet interbedded argillaceous limestone and olive gray claystone. Represents a transition from a predominately carbonate environment to a muddier marine environment.

Nealmont Formation:
270 feet thick in the northern valley, 256 feet thick on Dolly Ridge. Predominately a thin, wavy to crinkly bedded, sublithographic limestone with clay partings. Bioclastic limestones occur in the upper 70 feet. The lower 50 feet, which is seldom exposed, is relatively argillaceous. Usually occurs in outcrops as thin slabs of blue gray weathered limestone float with prominent buff colored burrows.

Black River Group

McGraw & McGlone Limestones

McGraw Limestone:
30 feet of medium to dark gray "granular" bioclastic to pelletic limestone. Medium to thick bedded, clay-free, more resistant to weathering, has granular appearance. Forms resistant ledges, provides an excellent marker for geologic mapping. Top of unit highly fossiliferous.

McGlone Limestone:
60 feet of interbedded pale to medium gray aphanitic limestone, and darker gray pelmicrite and bioclastic limestone. Forms resistant ledges. Top of unit is highly fossiliferous.

Big Valley Formation

Benbolt Member:
Medium to dark gray, somewhat argillaceous, silty limestone. Silty, fossiliferous in parts. 30 feet thick in the valley.

Ward Cove Member:
Dark gray to black, silty, argillaceous, pyritic limestone, with interbedded dark shale. 20 feet thick in the valley.

Lincolnshire Limestone
Predominantly dark gray, somewhat argillaceous pelletal limestone with scattered black chert nodules. About 30 feet thick in the valley. The Lincolnshire grades upward into the argillaceous knobby limestone and interbedded dark shale of the lower Big Valley Formation

New Market Limestone
Pure aphanitic limestone. Purest limestone formed in the study area. Pale to medium gray (dove-gray vaughnite), normally massive to thick bedded. Sparsely fossiliferous. Maclurite and orthoconic cephalopods in the upper part.

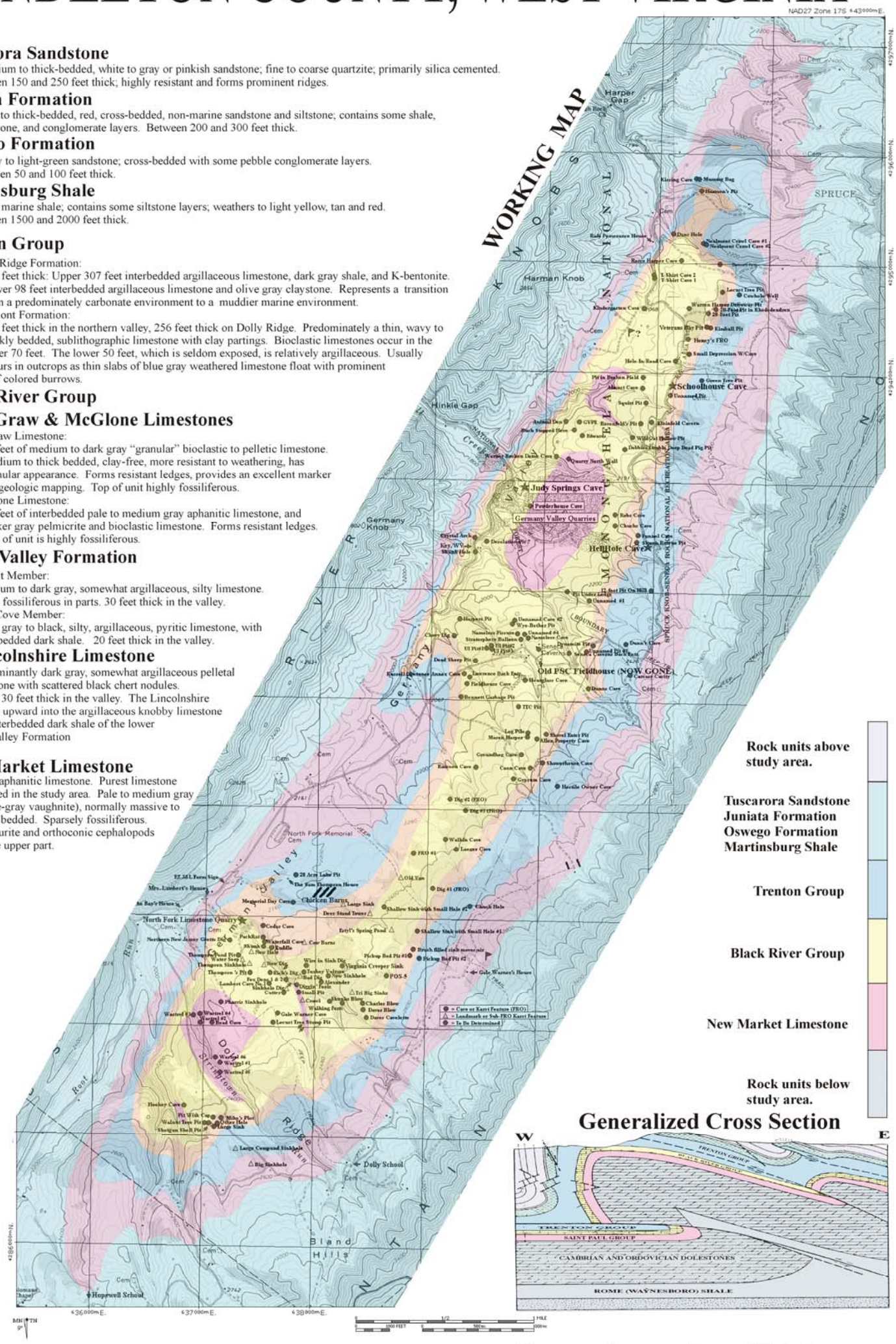
WORKING MAP
NAD27 Zone 17S
Harper Gap
Harman Knob
Hinkle Gap
Germany Knob
Judy Springs Cave
Helltole Cave
Old PSC Fieldhouse (NOW GONE)
Schoolhouse Cave
Germany Valley Quarries
North Fork Limestone Quarry
Chicken Barns
Dolly Ridge
Bland Hills
Hopewell School
Rock Ridge
Rock Ridge Ridge
Rock Ridge Run
Rock Ridge Trail
Rock Ridge Trail Head
Rock Ridge Trail Head Parking
Rock Ridge Trail Head Parking Lot
Rock Ridge Trail Head Parking Lot Entrance
Rock Ridge Trail Head Parking Lot Entrance Road
Rock Ridge Trail Head Parking Lot Entrance Road Sign
Rock Ridge Trail Head Parking Lot Entrance Road Sign Post
Rock Ridge Trail Head Parking Lot Entrance Road Sign Post Base
Rock Ridge Trail Head Parking Lot Entrance Road Sign Post Base Concrete
Rock Ridge Trail Head Parking Lot Entrance Road Sign Post Base Concrete Footing
Rock Ridge Trail Head Parking Lot Entrance Road Sign Post Base Concrete Footing Hole
Rock Ridge Trail Head Parking Lot Entrance Road Sign Post Base Concrete Footing Hole Bottom
Rock Ridge Trail Head Parking Lot Entrance Road Sign Post Base Concrete Footing Hole Bottom Rock
Rock Ridge Trail Head Parking Lot Entrance Road Sign Post Base Concrete Footing Hole Bottom Rock Ridge
Rock Ridge Trail Head Parking Lot Entrance Road Sign Post Base Concrete Footing Hole Bottom Rock Ridge Run
Rock Ridge Trail Head Parking Lot Entrance Road Sign Post Base Concrete Footing Hole Bottom Rock Ridge Run Trail
Rock Ridge Trail Head Parking Lot Entrance Road Sign Post Base Concrete Footing Hole Bottom Rock Ridge Run Trail Head
Rock Ridge Trail Head Parking Lot Entrance Road Sign Post Base Concrete Footing Hole Bottom Rock Ridge Run Trail Head Parking
Rock Ridge Trail Head Parking Lot Entrance Road Sign Post Base Concrete Footing Hole Bottom Rock Ridge Run Trail Head Parking Lot
Rock Ridge Trail Head Parking Lot Entrance Road Sign Post Base Concrete Footing Hole Bottom Rock Ridge Run Trail Head Parking Lot Entrance
Rock Ridge Trail Head Parking Lot Entrance Road Sign Post Base Concrete Footing Hole Bottom Rock Ridge Run Trail Head Parking Lot Entrance Road
Rock Ridge Trail Head Parking Lot Entrance Road Sign Post Base Concrete Footing Hole Bottom Rock Ridge Run Trail Head Parking Lot Entrance Road Sign
Rock Ridge Trail Head Parking Lot Entrance Road Sign Post Base Concrete Footing Hole Bottom Rock Ridge Run Trail Head Parking Lot Entrance Road Sign Post
Rock Ridge Trail Head Parking Lot Entrance Road Sign Post Base Concrete Footing Hole Bottom Rock Ridge Run Trail Head Parking Lot Entrance Road Sign Post Base
Rock Ridge Trail Head Parking Lot Entrance Road Sign Post Base Concrete Footing Hole Bottom Rock Ridge Run Trail Head Parking Lot Entrance Road Sign Post Base Concrete
Rock Ridge Trail Head Parking Lot Entrance Road Sign Post Base Concrete Footing Hole Bottom Rock Ridge Run Trail Head Parking Lot Entrance Road Sign Post Base Concrete Footing
Rock Ridge Trail Head Parking Lot Entrance Road Sign Post Base Concrete Footing Hole Bottom Rock Ridge Run Trail Head Parking Lot Entrance Road Sign Post Base Concrete Footing Hole
Rock Ridge Trail Head Parking Lot Entrance Road Sign Post Base Concrete Footing Hole Bottom Rock Ridge Run Trail Head Parking Lot Entrance Road Sign Post Base Concrete Footing Hole Bottom
Rock Ridge Trail Head Parking Lot Entrance Road Sign Post Base Concrete Footing Hole Bottom Rock Ridge Run Trail Head Parking Lot Entrance Road Sign Post Base Concrete Footing Hole Bottom Rock
Rock Ridge Trail Head Parking Lot Entrance Road Sign Post Base Concrete Footing Hole Bottom Rock Ridge Run Trail Head Parking Lot Entrance Road Sign Post Base Concrete Footing Hole Bottom Rock Ridge
Rock Ridge Trail Head Parking Lot Entrance Road Sign Post Base Concrete Footing Hole Bottom Rock Ridge Run Trail Head Parking Lot Entrance Road Sign Post Base Concrete Footing Hole Bottom Rock Ridge Run
Rock Ridge Trail Head Parking Lot Entrance Road Sign Post Base Concrete Footing Hole Bottom Rock Ridge Run Trail Head Parking Lot Entrance Road Sign Post Base Concrete Footing Hole Bottom Rock Ridge Run Trail
Rock Ridge Trail Head Parking Lot Entrance Road Sign Post Base Concrete Footing Hole Bottom Rock Ridge Run Trail Head Parking Lot Entrance Road Sign Post Base Concrete Footing Hole Bottom Rock Ridge Run Trail Head
Rock Ridge Trail Head Parking Lot Entrance Road Sign Post Base Concrete Footing Hole Bottom Rock Ridge Run Trail Head Parking Lot Entrance Road Sign Post Base Concrete Footing Hole Bottom Rock Ridge Run Trail Head Parking
Rock Ridge Trail Head Parking Lot Entrance Road Sign Post Base Concrete Footing Hole Bottom Rock Ridge Run Trail Head Parking Lot Entrance Road Sign Post Base Concrete Footing Hole Bottom Rock Ridge Run Trail Head Parking Lot
Rock Ridge Trail Head Parking Lot Entrance Road Sign Post Base Concrete Footing Hole Bottom Rock Ridge Run Trail Head Parking Lot Entrance Road Sign Post Base Concrete Footing Hole Bottom Rock Ridge Run Trail Head Parking Lot Entrance
Rock Ridge Trail Head Parking Lot Entrance Road Sign Post Base Concrete Footing Hole Bottom Rock Ridge Run Trail Head Parking Lot Entrance Road Sign Post Base Concrete Footing Hole Bottom Rock Ridge Run Trail Head Parking Lot Entrance Road
Rock Ridge Trail Head Parking Lot Entrance Road Sign Post Base Concrete Footing Hole Bottom Rock Ridge Run Trail Head Parking Lot Entrance Road Sign Post Base Concrete Footing Hole Bottom Rock Ridge Run Trail Head Parking Lot Entrance Road Sign
Rock Ridge Trail Head Parking Lot Entrance Road Sign Post Base Concrete Footing Hole Bottom Rock Ridge Run Trail Head Parking Lot Entrance Road Sign Post Base Concrete Footing Hole Bottom Rock Ridge Run Trail Head Parking Lot Entrance Road Sign Post
Rock Ridge Trail Head Parking Lot Entrance Road Sign Post Base Concrete Footing Hole Bottom Rock Ridge Run Trail Head Parking Lot Entrance Road Sign Post Base Concrete Footing Hole Bottom Rock Ridge Run Trail Head Parking Lot Entrance Road Sign Post Base
Rock Ridge Trail Head Parking Lot Entrance Road Sign Post Base Concrete Footing Hole Bottom Rock Ridge Run Trail Head Parking Lot Entrance Road Sign Post Base Concrete Footing Hole Bottom Rock Ridge Run Trail Head Parking Lot Entrance Road Sign Post Base Concrete
Rock Ridge Trail Head Parking Lot Entrance Road Sign Post Base Concrete Footing Hole Bottom Rock Ridge Run Trail Head Parking Lot Entrance Road Sign Post Base Concrete Footing Hole Bottom Rock Ridge Run Trail Head Parking Lot Entrance Road Sign Post Base Concrete Footing
Rock Ridge Trail Head Parking Lot Entrance Road Sign Post Base Concrete Footing Hole Bottom Rock Ridge Run Trail Head Parking Lot Entrance Road Sign Post Base Concrete Footing Hole Bottom Rock Ridge Run Trail Head Parking Lot Entrance Road Sign Post Base Concrete Footing Hole
Rock Ridge Trail Head Parking Lot Entrance Road Sign Post Base Concrete Footing Hole Bottom Rock Ridge Run Trail Head Parking Lot Entrance Road Sign Post Base Concrete Footing Hole Bottom Rock Ridge Run Trail Head Parking Lot Entrance Road Sign Post Base Concrete Footing Hole Bottom
Rock Ridge Trail Head Parking Lot Entrance Road Sign Post Base Concrete Footing Hole Bottom Rock Ridge Run Trail Head Parking Lot Entrance Road Sign Post Base Concrete Footing Hole Bottom Rock Ridge Run Trail Head Parking Lot Entrance Road Sign Post Base Concrete Footing Hole Bottom Rock
Rock Ridge Trail Head Parking Lot Entrance Road Sign Post Base Concrete Footing Hole Bottom Rock Ridge Run Trail Head Parking Lot Entrance Road Sign Post Base Concrete Footing Hole Bottom Rock Ridge Run Trail Head Parking Lot Entrance Road Sign Post Base Concrete Footing Hole Bottom Rock Ridge
Rock Ridge Trail Head Parking Lot Entrance Road Sign Post Base Concrete Footing Hole Bottom Rock Ridge Run Trail Head Parking Lot Entrance Road Sign Post Base Concrete Footing Hole Bottom Rock Ridge Run Trail Head Parking Lot Entrance Road Sign Post Base Concrete Footing Hole Bottom Rock Ridge Run
Rock Ridge Trail Head Parking Lot Entrance Road Sign Post Base Concrete Footing Hole Bottom Rock Ridge Run Trail Head Parking Lot Entrance Road Sign Post Base Concrete Footing Hole Bottom Rock Ridge Run Trail Head Parking Lot Entrance Road Sign Post Base Concrete Footing Hole Bottom Rock Ridge Run Trail
Rock Ridge Trail Head Parking Lot Entrance Road Sign Post Base Concrete Footing Hole Bottom Rock Ridge Run Trail Head Parking Lot Entrance Road Sign Post Base Concrete Footing Hole Bottom Rock Ridge Run Trail Head Parking Lot Entrance Road Sign Post Base Concrete Footing Hole Bottom Rock Ridge Run Trail Head
Rock Ridge Trail Head Parking Lot Entrance Road Sign Post Base Concrete Footing Hole Bottom Rock Ridge Run Trail Head Parking Lot Entrance Road Sign Post Base Concrete Footing Hole Bottom Rock Ridge Run Trail Head Parking Lot Entrance Road Sign Post Base Concrete Footing Hole Bottom Rock Ridge Run Trail Head Parking
Rock Ridge Trail Head Parking Lot Entrance Road Sign Post Base Concrete Footing Hole Bottom Rock Ridge Run Trail Head Parking Lot Entrance Road Sign Post Base Concrete Footing Hole Bottom Rock Ridge Run Trail Head Parking Lot Entrance Road Sign Post Base Concrete Footing Hole Bottom Rock Ridge Run Trail Head Parking Lot

Three rivers drain the county; the North Fork of the South Branch of the Potomac River, the South Branch of the Potomac River, and the South Fork of the South Branch of the Potomac River (Figure 7). The three rivers all flow towards the North or Northeast. The regional drainage is trellis pattern, but at the local scale it is dendritic in nature (Dasher, 2001). The North Fork of the South Branch of the Potomac River runs adjacently north of Germany Valley (Figure 8). Pendleton County has 62 reported springs, 7 of which have recorded discharges of 3,800 liters per minute or greater (Jones, 1997). Judy Spring is the only major spring in Germany Valley. Discharge data for it is unknown (McColloch, 1986). A cave exists at the orifice of Judy Spring (Judy Springs Cave). Several attempts to dive and survey the cave have been made. No evidence has been found that the cave connects to Hellhole, but it has been widely suggested (Brace, 2003). Surveys of Judy Springs Cave indicate that greater than 1.2 km of passage exist and continue towards Hellhole and Schoolhouse Cave (Wilson, 1977).

The water table was encountered in Hellhole at a depth of approximately 130 meters (GVKS, 2004). The cave has two perennial streams at this depth.

Larry Kisamore, a local resident with property overlying Hellhole, owns a domestic water well installed in an aquifer higher than the (cave) water table. The well is about 30 meters deep (Appendix A). According to Larry Kisamore, there also exist two springs that were historically used for old dwellings. South of Hellhole, more centrally located in the valley, is Danny Kisamore's well. He reports that the depth of the well is 136 meters (Kisamore, 2005). Well reports for the vicinity of the study area are difficult

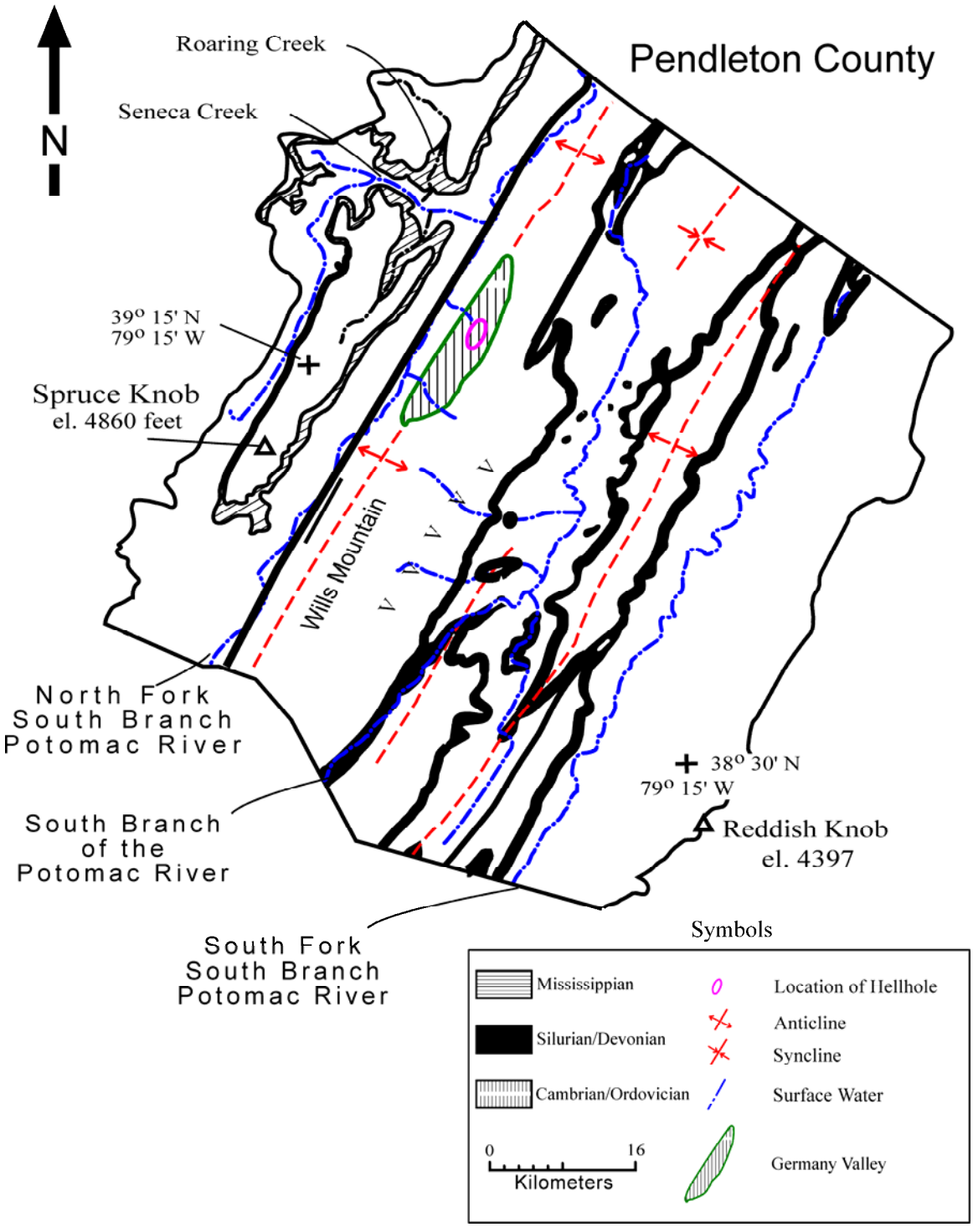

Figure 7. Geology and hydrography of Pendleton County, courtesy of Greg Springer.

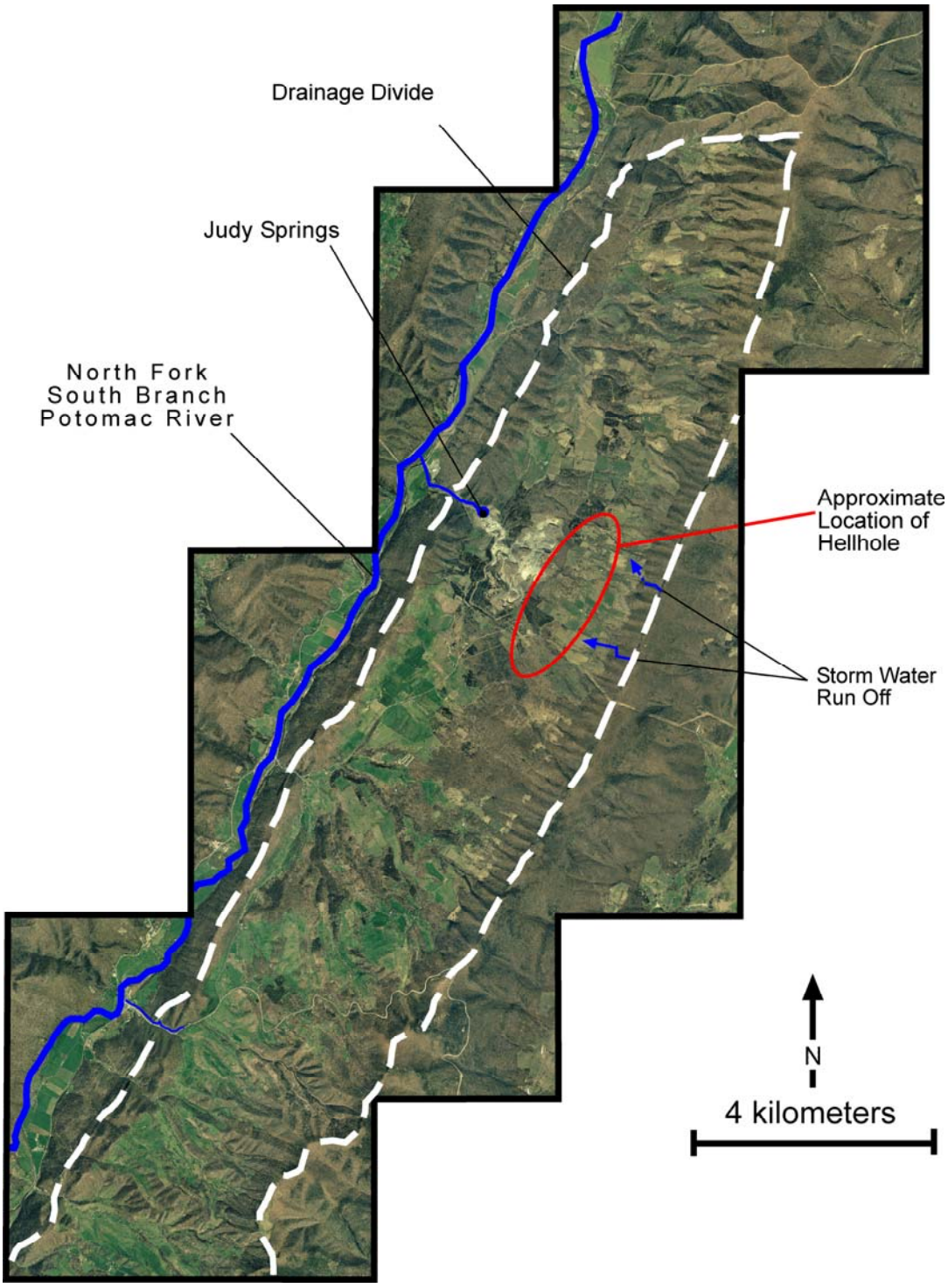

Figure 8. Color orthophotograph of the enclosed Germany Valley drainage basin. Base data from West Virginia GIS Technical Center, (2003).

to acquire because West Virginia did not require well reports on new wells until 1985. Most residents of the valley settled prior to 1985.

Germany Valley has a long history of human habitation. There is record of European settlement since the 1700's. American Indians resided in the valley long before then. During the Civil War, saltpeter was mined from the local caves to be used in the manufacture of gunpowder (Chapman, 1970). In addition, soldiers used the caves for storage of pillaged money and property. One cave of particular interest is Schoolhouse Cave, which may be the only cave in the state that was mined for saltpeter only by the Union (Dasher, 2000). Schoolhouse Cave also may be the oldest saltpeter mine in West Virginia, dating back to French and Indian War times (Dasher, 2000). Cave exploration began in this area in the 1940's. Professor Albert Krause, a minister, first explored several caves in the valley (Dasher, 2000). Since then many other caves have been discovered.

Hellhole is the largest and deepest known cave in the valley (Figure 9 and 10). Also, it is centrally located near the axis of the overturned Wills Mountain anticline. The cave has multiple levels that have potentially preserved important paleohydrologic information. Evidence of structural deformation is also found in the cave. The structural and hydrologic influences are recorded in the limestone walls of the cave.

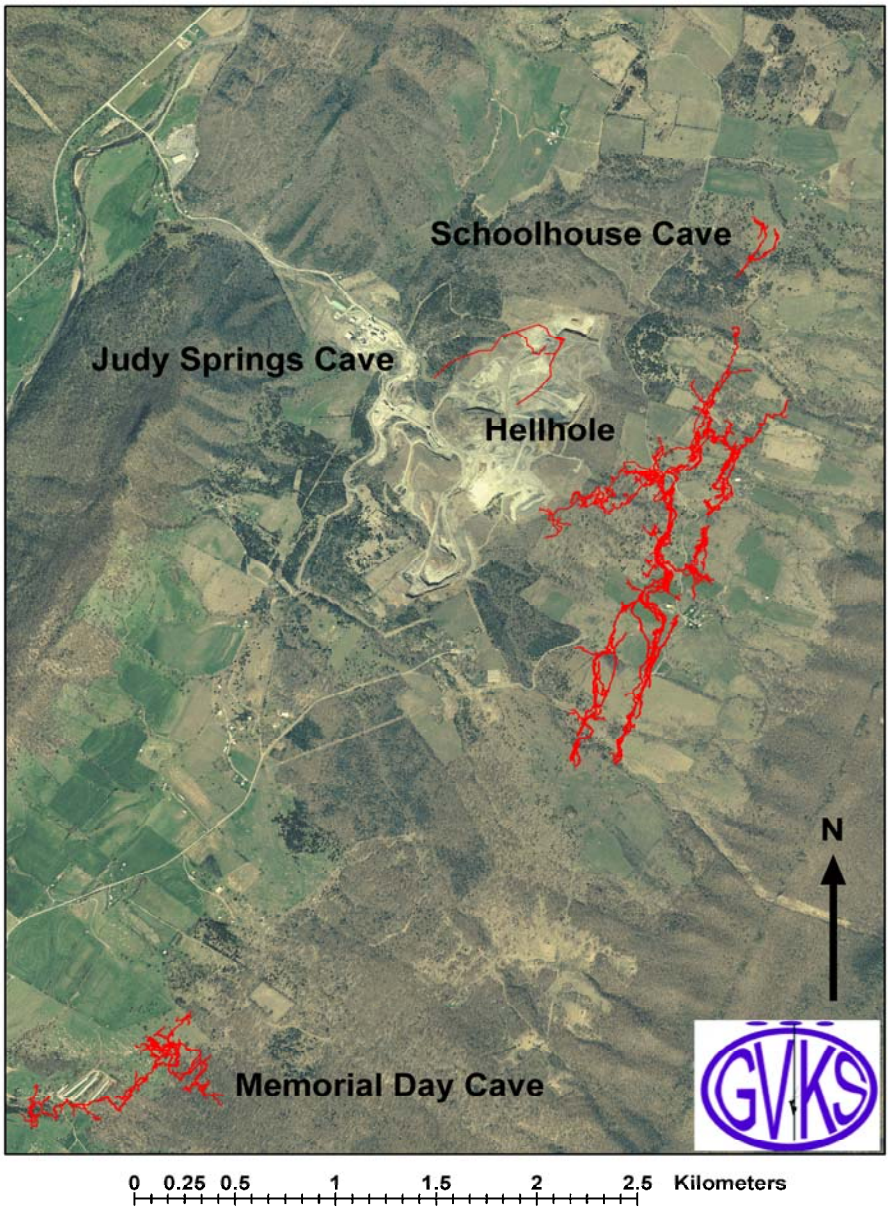

Figure 9. Color orthophotograph of the Germany Valley area with maps of major caves shown in red. Base data from West Virginia GIS Technical Center, (2003). Cave survey data courtesy of GVKS, (2004).

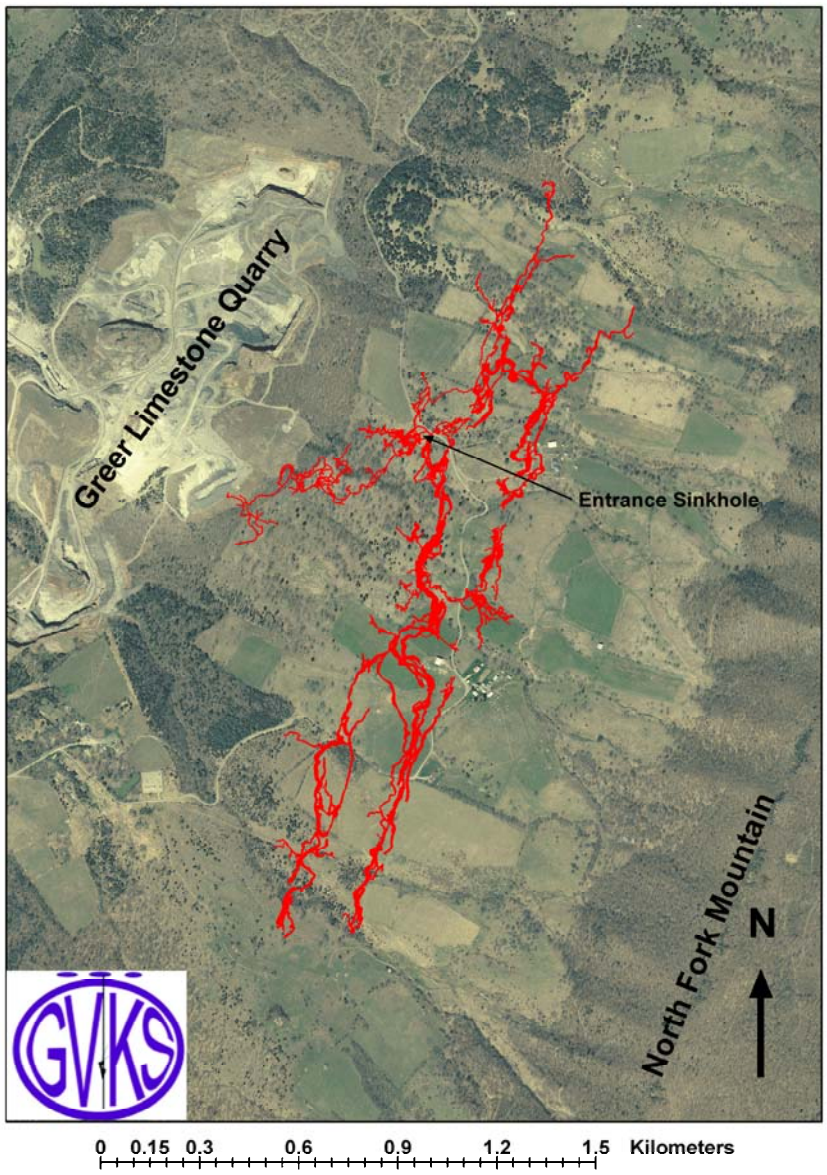

Figure 10. Color orthophotograph of vicinity and map of Hellhole. Base data from West Virginia GIS Technical Center, (2003). Cave survey data courtesy of GVKS, (2004).

CHAPTER III

INVESTIGATION OF STRUCTURAL GEOLOGY

Introduction

Evaluation of the structure of the bedrock allows the comparison of this cave with other known caves in similar settings. Also the structural investigation yields information of the strike and dip of the bedrock, locations of major features, and other structural controls of Hellhole.

The Wills Mountain Anticline has three primary structural levels according to Perry (1975). The following description is derived from his work. The upper level consists of upper Silurian, Devonian, and upper Ordovician sandstone, mudstone, shale and limestone. This level is mostly folded. The middle level consists of thrust-faulted Ordovician and Cambrian carbonate sequences. These massive dolostone sequences were tectonically stacked in four major thrust blocks. The lowest level is a lower Cambrian strata that overlie a probable gneissic basement.

According to a study in structurally controlled valleys of Pennsylvania by Deike (1969), there is a high frequency of joints between N60°E and N70°E that parallel the anticline fold axes. As a group, caves in these areas develop passages in two orientations, N65°E and N25°W. These are also the azimuths of strike and dip of the strata in those parts of the Valley and Ridge Province (Deike, 1969). The Wills Mountain Anticline axis

in Germany Valley is oriented N30°E. Dip direction on the East limb (study area) is S60°E. Anticipated cave passage direction would mimic these orientations.

Hellhole is bounded on the North and South by fracture sets that are perpendicular to the axis of the anticline (Brace, 2003). The Fiddler's Green fracture set is to the south, and the Wildcat Hollow fracture set to the north (Figure 11). The fracture sets can be recognized by faults in the drainage ways in each hollow. The Wildcat Hollow fracture set was discovered and named only a few years ago by members of the Germany Valley Karst Survey.

Methods

Multiple strike and dip measurements were taken in the cave (Appendix B). Measurements were difficult to obtain due to lack of exposed bedding plane surfaces, and poor accessibility of good bedding plane surfaces. Positions of measurements were selected based upon availability. Additional strike and dip measurements were taken along the road above the cave. Measurements were taken with a Brunton Pocket Transit and a Suunto Tandem compass. Observable structural features such as folds and faults were visually identified in cave during multiple examinations. These features were sought out in order to determine if they influenced cave development.

Strike data were compiled to make rose diagrams using the program ROCKWORKS (Rockware, 2002). In addition, a rose diagram was constructed using the program COMPASS (Fountainware, 2003) by extracting the frequency of the azimuth of cave passage segments (length-weighted) from cave survey data. The rose diagrams

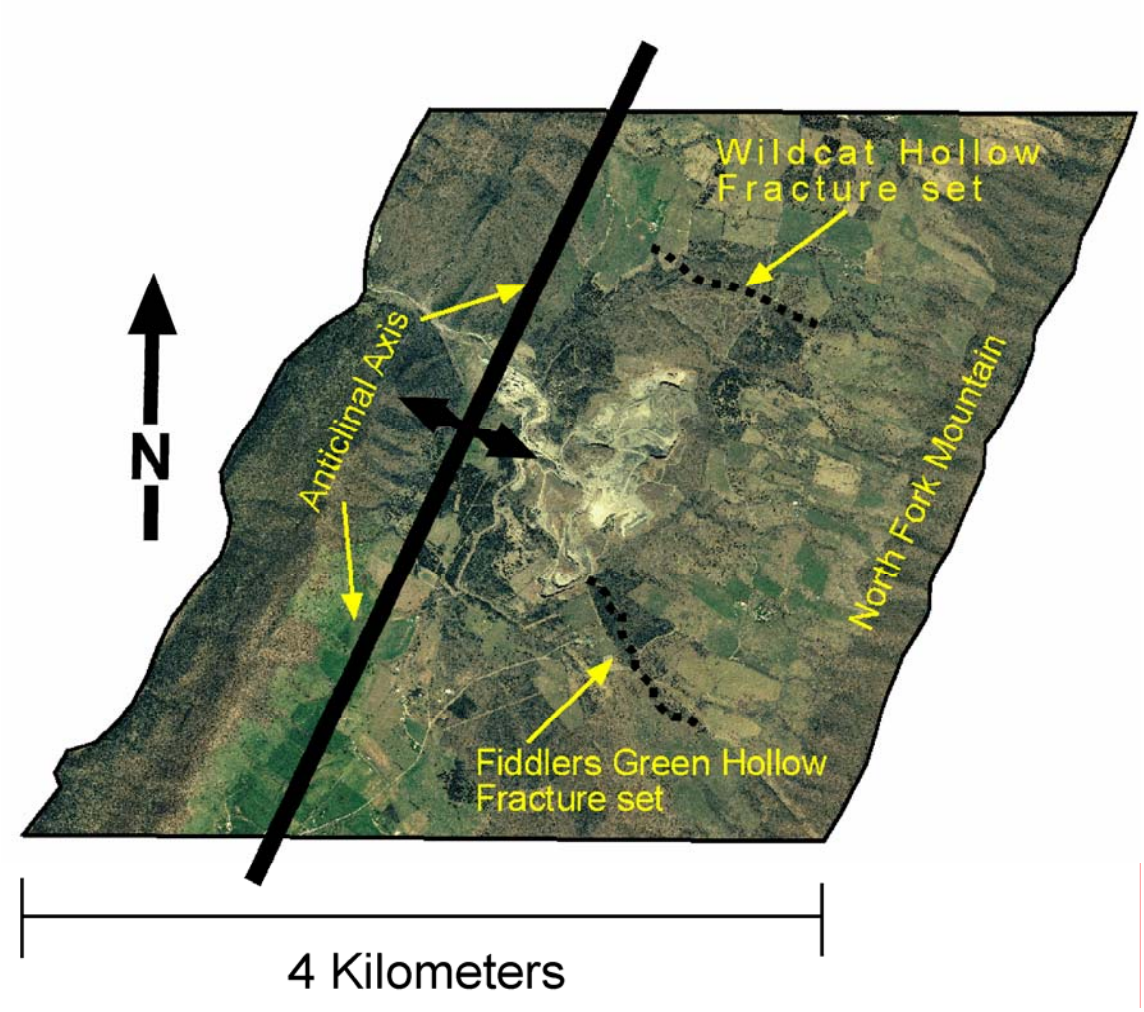

Figure 11. Terrain visualization with major structural features in the study area. Base data from West Virginia GIS Technical Center, (2003)

were then used to evaluate the association between passage orientation and bedrock strike.

Results

Figure 12a shows strikes measured on bedding planes within Hellhole. Figure 12b is composed of strikes of fault surfaces within Hellhole. Seven measurements were recorded from this diagram. Figure 12c is composed of strikes of bedding planes on the surface, above Hellhole. Three measurements were recorded for this diagram, one to the North of the cave, one to the South, and one more centrally located. It should be noted that the northern-most and southern-most measurements were collected near Wildcat Hollow fracture set and Fiddlers Green Hollow fracture set, respectively.

Figure 13 is the length-weighted compilation of cave passage directions (Figure 11). A total of nearly 38 kilometers of compass and tape survey was used. The rose diagram shows passage in all directions, but the strongest direction is at N25ºE. This is the primary direction of cave passage, and the data set shows that the majority of passage developed between N10ºE and N50ºE.

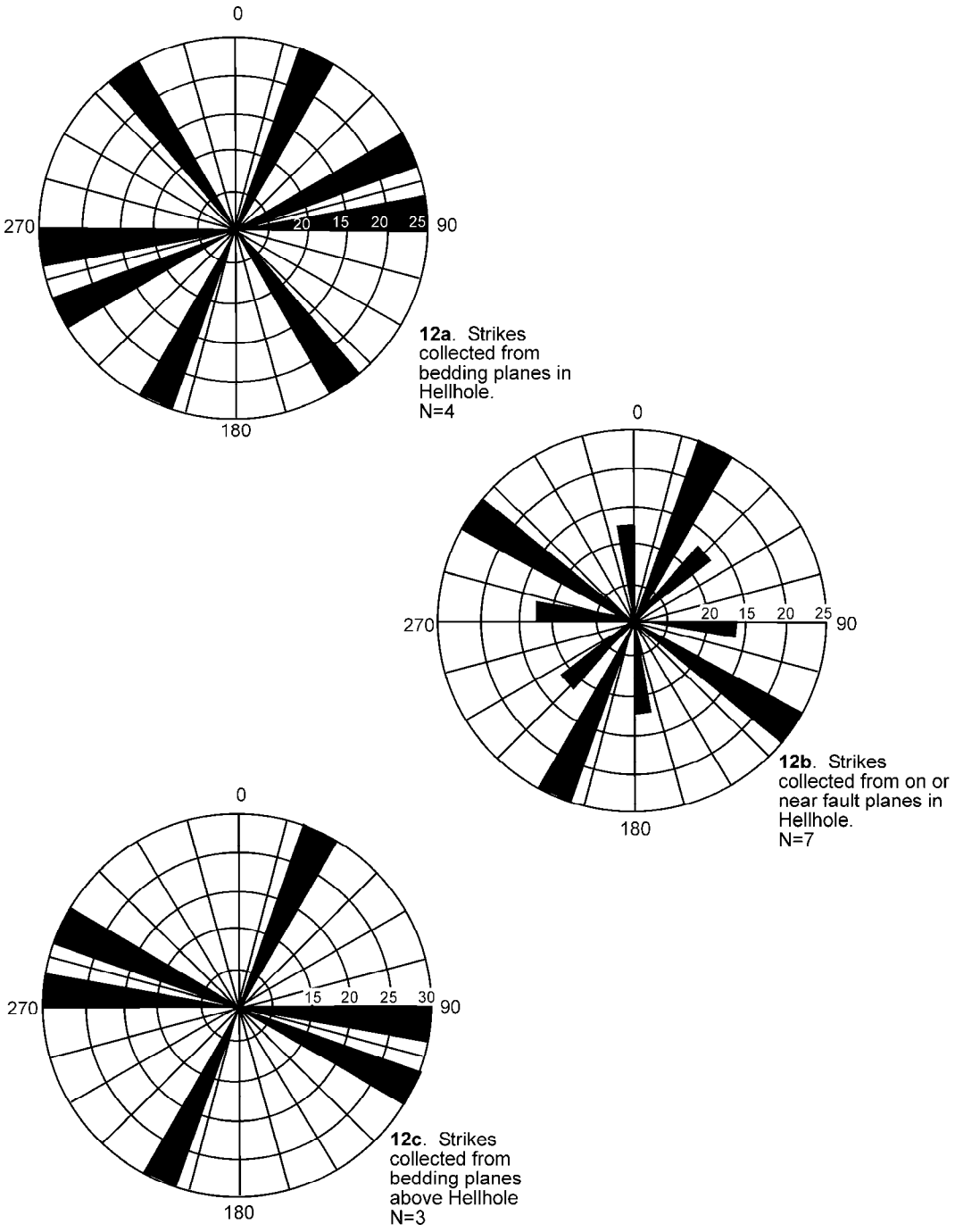

Figure 12. Rose diagrams of strike in Germany Valley. Figures a through c were compiled using ROCKWORKS (Rockware, 2002). Numbers on radial axis are percent of total measurements.

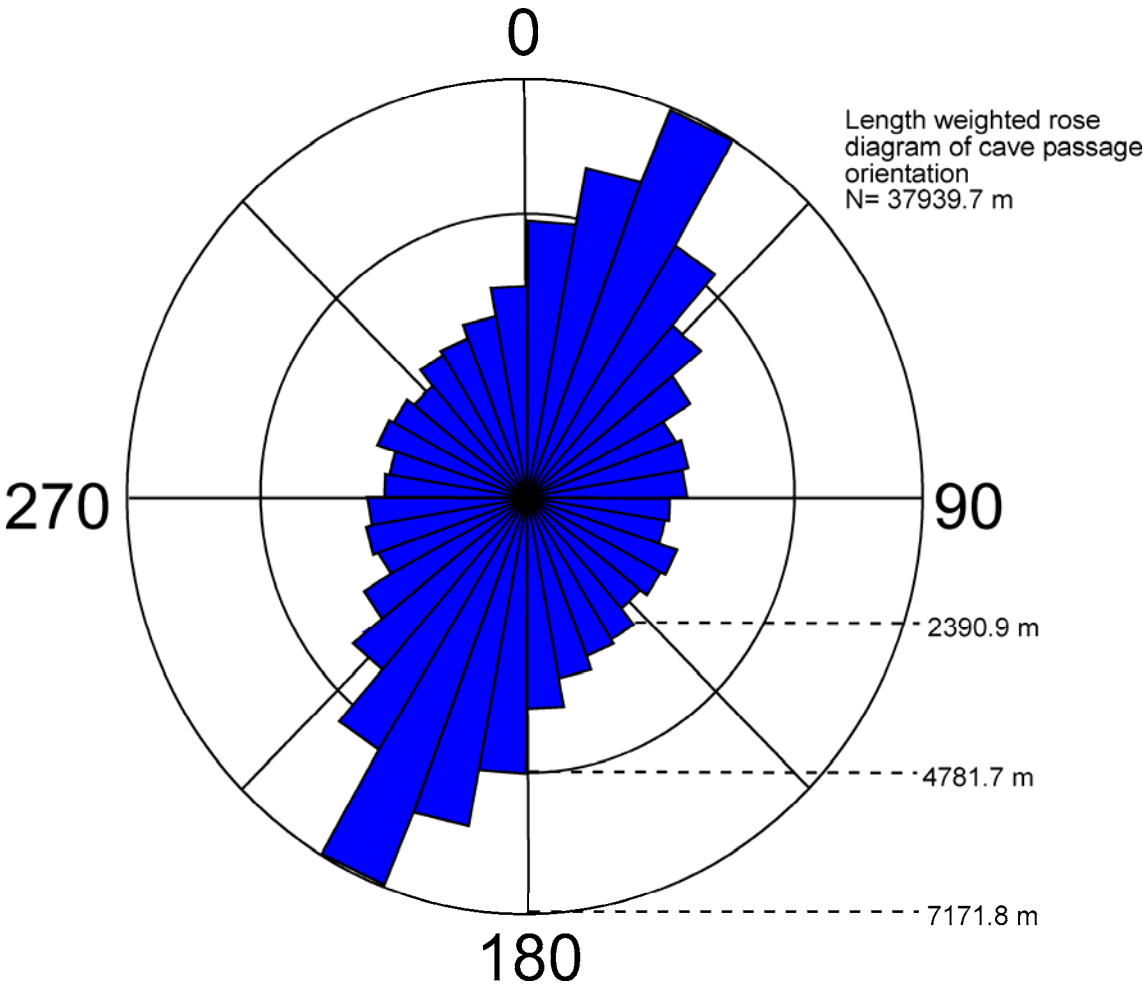

Figure 13. Rose diagram of Hellhole cave passage direction. Derived from survey data, courtesy of GVKS, (2004) compiled using COMPASS (Fountainware, 2003).

Several faults were observed in the cave (Figure 14). None of the faults, or folding related to the faults, appears to have had a large influence on passage location. Passages developed across the structures without change of direction or shape. In the trunk passage called Bob's Big Break Borehole (Figure 14, position T, and Figure 15), a fault exists with associated folding. Cave passage directly cuts across it. The fault is only observable on west side of the passage (the other side is covered in breakdown). A fault exists at the base of the quadruple dome complex (four joined vertical shafts) at the end of HSB survey (Figure 14, position L). The fault, which is a thrust, is present on either side of the passage. The conduit formed across it, and terminates in muddy breakdown. A thrust fault exists just past the Window Dome (Figure 14, position E). The fault is only observable on one side of passage (the other side is covered with secondary calcite growth). The fault does not seem to be a factor in the cave development. In the Historical Section along Dartt Canyon (Figure 14, position B), a fault can be observed along one side of the passage. Passage development was not affected by the feature. In the Northwest portion of the cave (Figure 14, position D), along the end of the DD survey, a fault cuts across the passage at an angle. The cave developed through the fault and in to a dome (vertical shaft) that ends in a mud plug. Also, along the Raccoon Passage (Figure 14, position C, and Figure 16) small faults were noted along the walls. Again, cave passage (shape, position) was not affected by presence of faulting.

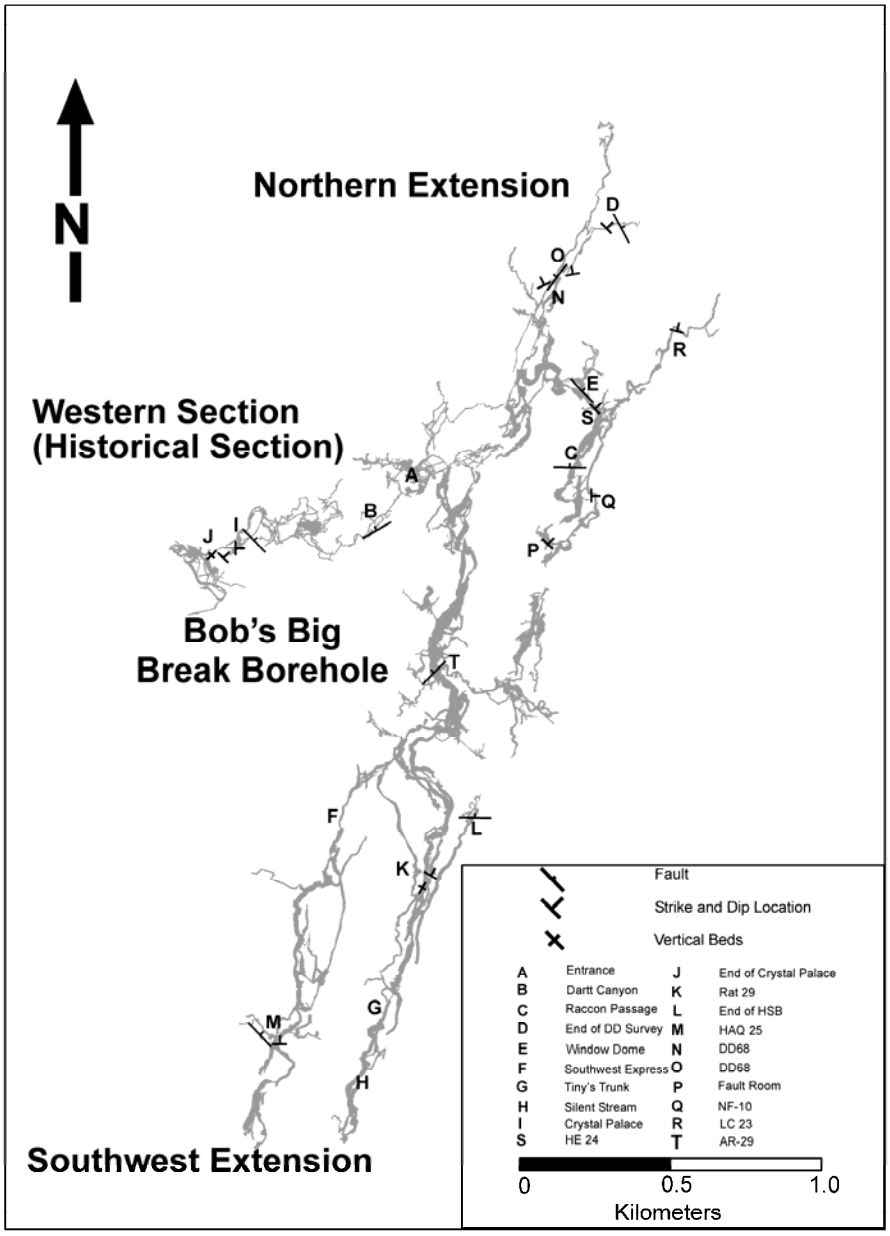

Figure 14. Map of the locations of faults and strike and dip measurements. Passage survey data courtesy of GVKS.

Figure 15. Photograph of a fault related fold in Bob's Big Break Borehole

Figure 16. Photograph of a fault related fold near Raccoon Passage

CHAPTER IV

CAVE SEDIMENT AND PALEOMAGNETIC INVESTIGATION

Introduction

Cave sediments contain valuable geologic information, often overlooked when evaluating cavern development. Sediments occur in most caves, and can either be autochthonous or allochthonous (Gunn, 2004). Autochthonous sediments are generated in the cave from the weathering of the limestone. Allochthonous sediments are generated outside of the cave and transported in. Determination of a source area of cave sediments can lead to a better understanding of the evolution of a cave (Haney, 2002). Sediments can indicate the environment and time in which a cave developed. Numerous investigations have been conducted using cave sediments to correlate sediment deposition with time (e.g. Schmidt, 1982). Schmidt's study of Mammoth Cave, Kentucky, was the first to date sediments using paleomagnetism (Culver and White, 2005).

Paleomagnetism is a tool that can be used to determine ages of sediments. Most sediments contain magnetic remanence. Clastic fluvial sediments commonly contain fine-grained magnetite and hematite. When deposited, the magnetic particles tend to settle under the influence of the Earth's gravitational force as well as the ambient magnetic field. The magnetic sedimentary grains are oriented to the magnetic North Pole at the time of deposition. During the course of the Earth's history, magnetic reversals of

the north and south poles have occured. Numerical age of the polarity changes is assigned by a variety of methods, resulting in a global magnetostratigraphy (Evans and Heller, 2003).

Units in the geomagnetic polarity timescale are measured in chrons and subchrons (Evans and Heller, 2003). Each chron is an interval of the timescale. Subchrons are polarity changes during a chron interval. Chrons are labeled C (Chron), 1 (Chron number), and polarity (n or r). Subchrons are labeled by the chron designation followed by a period, subchron number (1), and the polarity (n or r). This timescale is associated with ocean floor records. In caves, the sediments can be analyzed and correlated to the global record. By correlation, a minimum age of the sediments can be determined.

Another nomenclature for the geomagnetic timescale utilizes names for the intervals and subintervals. Epochs are the primary intervals with the subintervals called events (Evans and Heller, 2003). Brunhes, Matuyama, Gauss, and Gilbert are the only named epochs. Jaramillo, Cobb Mountain, Olduvai, Reunion, Keana, Mammoth, Cochiti, Nunivak, Sidufjall, and Thvera are the only named events (Evans and Heller, 2003). This system provides names for applicable geomagnetic timescale intervals. The use of this timescale is usually associated with terrestrial records.

The first chron (C1n) coincides with the Brunhes Epoch. C1r.1r is equivalent to the reversed polarity interval between the Brunhes Epoch and the Jarramillo event. C1r.1n coincides with the Jaramillo event. C1r.2r represents the reversed polarity

interval between the Jarramillo event and the Cobb Mountain event. C1r.2n represents the Cobb Mountain event during the Matuyama epoch on the terrestrial time scale.

Methods

A series of 22 reconnaissance visits to the cave were made. During this time about 38 kilometers of cave passages were inspected, in order to find the most useful sampling location. Based upon this, samples were collected at an area of the cave known as Sand Hill (Figure 17). This area of the cave was chosen because it has a thick sequence of sediments, and therefore could provide the most complete stratigraphy. 14 pairs of samples were collected for a total of 28 samples. Photographs were taken and a measured stratigraphic column was constructed at the same time that samples were collected. Sampling intervals were based on vertical distance from the previous sample and changes in sediment characteristics in the sedimentary section.

Sample horizon selection was dependent upon access to undisturbed sediments. Most of the deposit was in place, or only a minor amount of excavation yielded undisturbed sediments. Sediments collected appeared to be in their original position, and with bedding still intact. The location revealed a thick exposure of sediments without requiring trenching. The major constituents of the slope consisted of silts, clays, and sands, with some trace gravel and calcareous clasts (fragments of speleothems).

Paired paleomagnetic samples were collected in labeled 8 mL plastic cubes following the methods of Sasowsky et al., (1995). Care was taken not to allow metal to contact any samples or subject the samples to any strong magnetic fields. The numbering

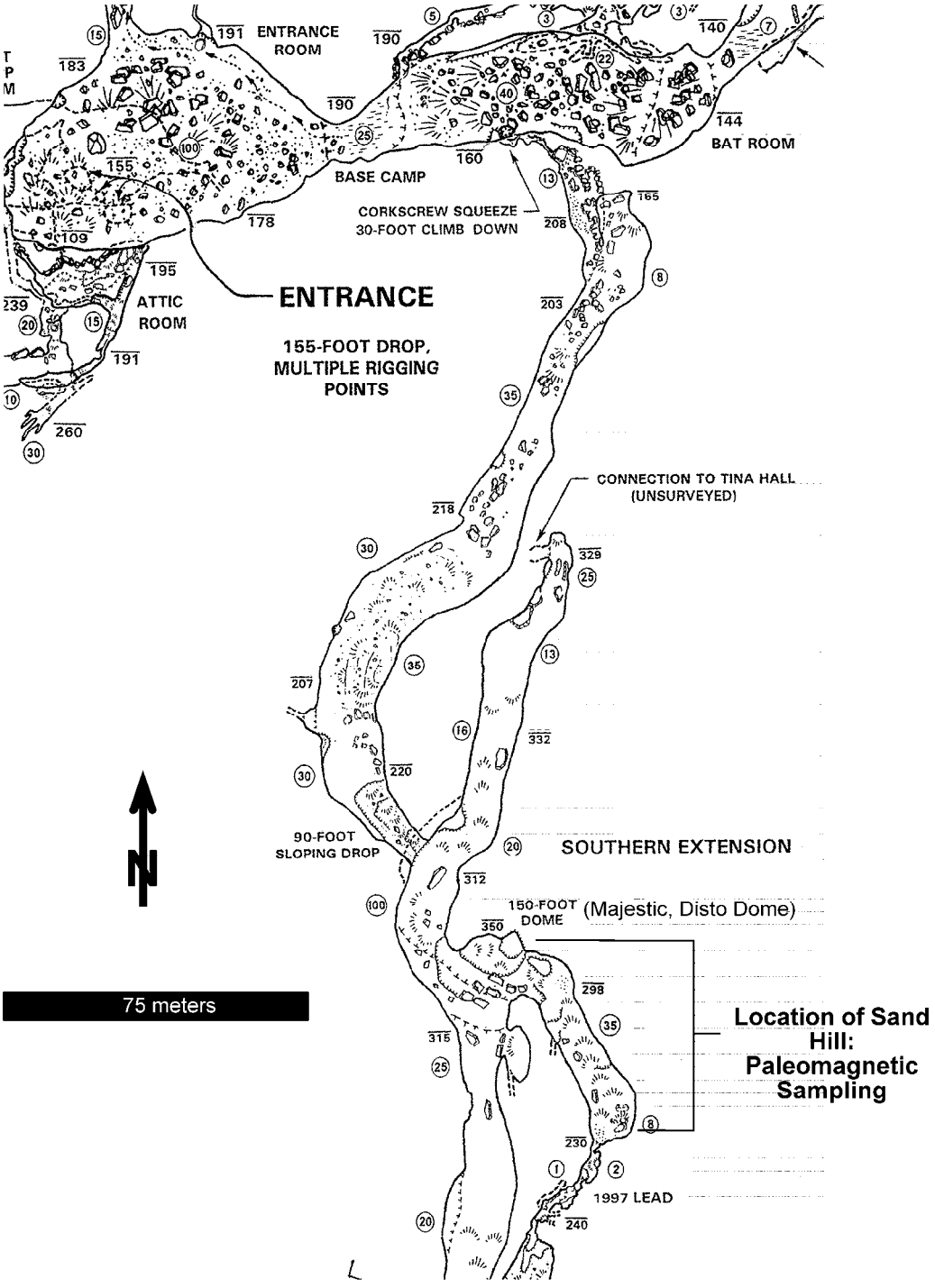

Figure 17. Map of a portion of Hellhole showing paleomagnetic sampling location. Map courtesy of Ed Devine (Dasher, 2001)

system for samples used the prefix “DCZ” followed by a sequential sample number beginning with 001 (DCZ001 through DCZ028). Sample cubes were marked with the identification prefix and an arrow to standardize the cube faces (axises). Strike, dip and tilt angle were then measured on each cube to provide its orientation for lab analysis (Appendix C). Photographs were taken of each sampling location, and locations were mapped on the stratigraphic column. In addition, three bulk sediment samples were also collected for descriptive analysis of the material.

Paleomagnetic samples were taken from the cave in zip lock bags and then refrigerated with a moist paper towel to maintain the sediment moisture. The samples were then brought to the University of Pittsburgh Paleomagnetic lab for analysis. The lab utilizes a large-bore SCT cryogenic magnetometer in a magnetically shielded room that reduces the Earth’s magnetic field strength to less than 2.5×10^{-4} millitesla (mT). Samples were subjected to various step-wise alternating field (AF) demagnetization levels depending on sample coercivity. Zijderveld diagrams (Appendix D) and Schimdt equal area pole plots were created to determine the vector of magnetic polarity for each sample. Samples were measured for magnetic susceptibility, the amount of magnetism per unit field (Evans and Heller, 2003) in two orientations (arrow on top, pointing out of coil; and arrow on front of cube, pointing downward) using a Sapphire Instruments SI-2 magnetic susceptibility instrument (Appendix E).

Bulk sediment samples were stored in gallon-sized zip lock bags until analyzed. Small grab samples were taken from each bulk sample bag to conduct the descriptive analysis. Descriptive analysis included visual analysis using a magnifier, washing to

determine basic lithology, and reactivity with hydrochloric acid (HCl). Visual analysis of the bulk sediment samples was conducted using a 16-power hand lens under a white fluorescent light. Basic lithology was determined after samples were washed to remove fine-grained sediment using water. An eyedropper with 10% HCl was used to slowly introduce acid to a portion of the sample to determine reactivity.

Results

Stratigraphic analysis of the sediment deposit revealed that the sediments consisted of a diverse range in sizes and lithologies from fine mud sized particles, fine to coarse sand, and gravel sized fragments of broken speleothems indicating changing flow velocities. Presently there is no running water in the passage and sediments in the section are all dry. However, the elevation of the bottom of the room (520 meters) is nearly the same elevation as Judy Spring (537 meters). In addition, the sedimentary deposits at Sand Hill are not flat lying. The sedimentary deposit is approximately 20 meters thick and has a strike of S32ºE and a dip of 22ºSW (Figures 18 through 20). Missing sections, or sections of the sedimentary section where no data could be collected were at 16.5 to 14.0 meters, 12.6 to 11.1 meters, and 8.5 to 7.2 meters from the top.

The bottom most sediments in the deposit at a depth from 20 to 17.7 meters consisted of white to tan laminated sand; some were encrusted with calcium carbonate. Above the laminated sand, from 17.7 to 16.5 meters, sediments consisted of planar sands interbedded with coarse sand and pebble sized gravel. The increase in grain size indicates an increase in paleoflow velocity. From 14.0 to 12.6 meters the sediments consisted of pebble-sized gravel to red mud in a fining upward sequence, indicating

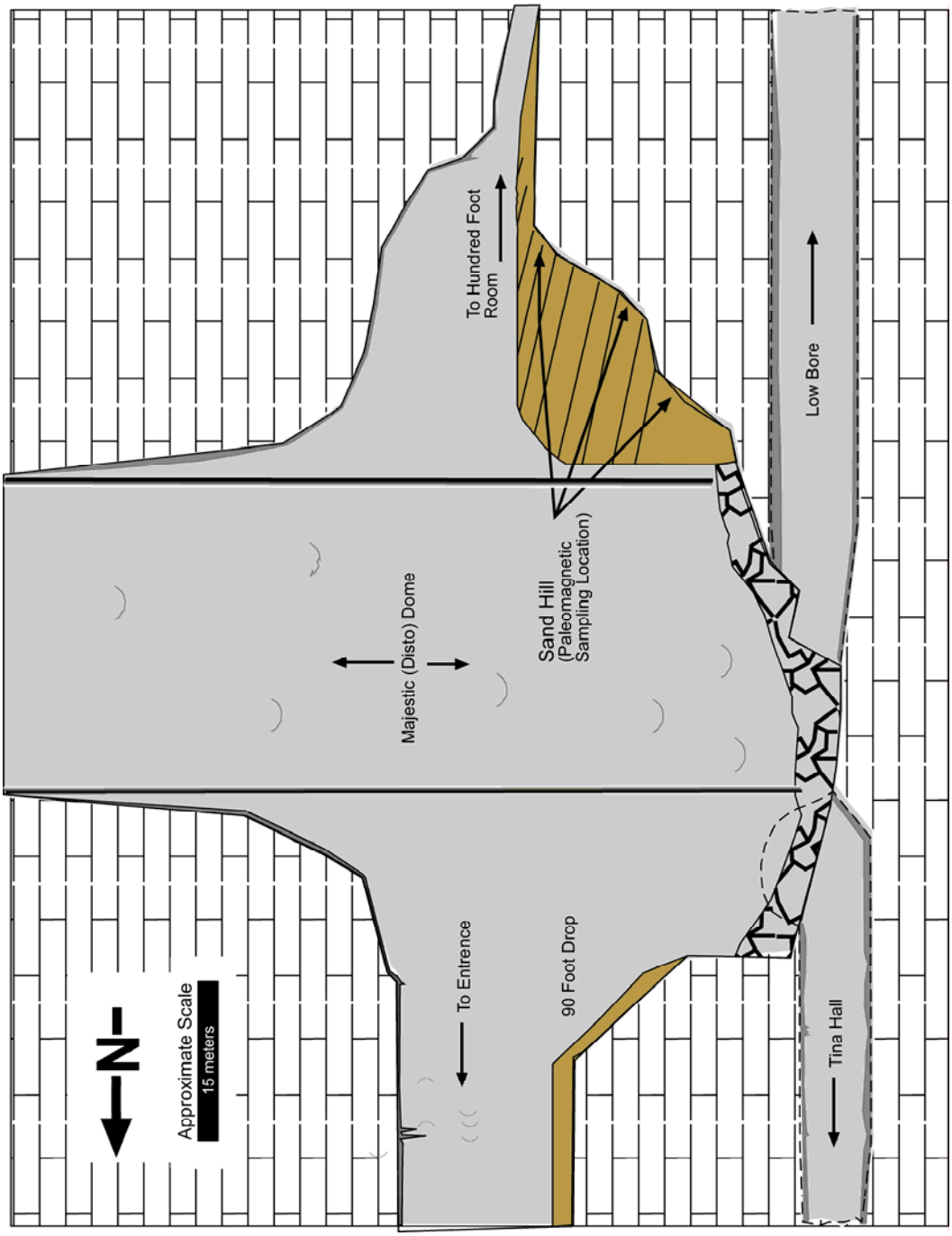

Figure 18. Schematic cross section of paleomagnetic sampling location. No vertical exaggeration.

Figure 19. Photographic overview of inclined beds of the Sand Hill. Interval shown is approximately the 5 to 8 meter level.

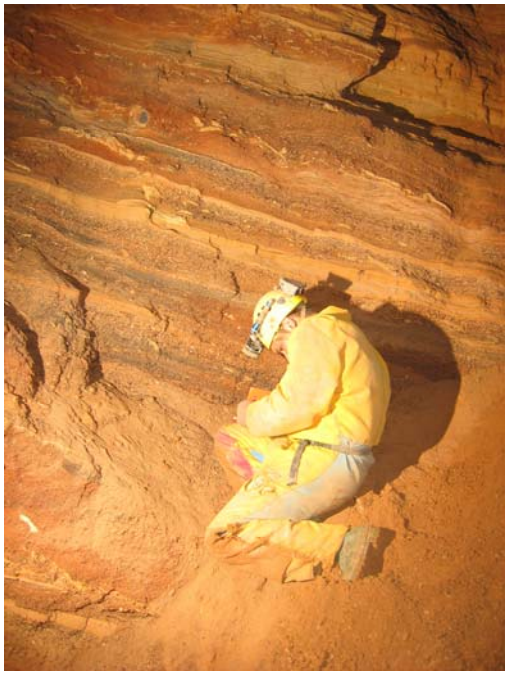

Figure 20. Photograph of the Sand Hill deposit at approximately the 4 to 5 meter interval.

a decrease in velocity. Sediments from 11.1 to 10.2 meters consisted of red and white fine-grained sand. At a depth of 10.2 to 8.5 meters gravel and broken speleothems interfingered with sand indicating a reciprocating intermediate to high paleoflow conditions was encountered. Tan silty clay indicating low velocity conditions was present at a depth of 6.3 meters. At an approximate depth of 5 meters there were trace amounts of gravel and broken speleothems, indicative of high flow conditions. Above the speleothems, was a coarsening upward sequence composed of clay, sand, and gravel, indicating a low flow velocity to an increase in velocity. At a depth of 4 meters, trace amounts of mud balls (mud peeled and curled from high velocity water) were encountered. The mud balls were overlain by fine white sand and interbedded subrounded gravel. Above the interbedded sand and gravel, interbedded gravel with silt and clay was noted to a depth of 2.9 meters. The topmost sediments in the deposit consisted of loose red silty sand that graded downward to tan silt, clay, and laminated mud to a depth of 2.2 meters. Cross stratification was noted at 10.3 meters, 5.0 meters and 4.1 meters. All the cross stratification indicated flow from south to north.

The first bulk sample was collected at a depth of 3.6 meters from the top. The bulk sample is composed of slightly cohesive subangular to subrounded tan (Munsell 5YR 6/6) and black, medium to coarse-grained sand, with some trace limestone gravel. The second bulk sample was collected 4.7 meters from the top. This bulk sample was composed of loose subrounded white and tan (Munsell 7.5YR 6/3) fine to medium grained sand with some subangular sandstone and shale gravel. The third bulk sample was collected 13.1 meters from the top. The bulk sample consisted of loose subrounded

gravel sized sandstone, chert, and shale fragments. The loose fragments were coated in a tan (Munsell 10YR 6/6) silt. None of the bulk samples effervesced when exposed to hydrochloric acid.

Most of the samples provided clear information about polarity. Zijderveld (1967) diagrams are presented in Appendix C. DCZ001 is a representative normal sample. The demagnetization path reveals an initial northward polarity and downward inclination that decreases toward the origin. Reversed polarity samples such as DCZ004 exhibit a low coercivity normal viscous natural remnant magnetization (NRM), which is removed during the demagnetization. Susceptibility of the samples ranged from 0.00000178 (DCZ026) to 0.0000589 (DCZ018) (Table 1).

Analysis of samples reveals a pattern of multiple polarities. Only samples that displayed a distinct normal or reversed declination and inclination were used for interpretation of age (Table 2). Schmidt equal area pole plots graph the characteristic remnant magnetic directions of the paleomagnetic samples (Figure 21). The pole plots indicate clustering of the samples exhibiting positive inclination (DCZ001, DCZ002, DCZ015, DCZ016, DCZ019, and DCZ020) in the northern hemisphere and clustering of the samples exhibiting a negative inclination (DCZ005 through DCZ007, DCZ010, DCZ011, DCZ013, DCZ014, DCZ022, and DCZ025 through DCZ028) in the southern hemisphere. In assigning age, the data of Cande and Kent, (1995) are used. The topmost normal polarity from samples DCZ001 and DCZ002 represents the present day normal polarity from 0.0 to 0.78 million years (C1n). The next oldest chron (C1r.1r) is represented in the reversed polarity samples DCZ005 through DCZ0014. C1r has an age

Table 1

Susceptibility of paleomagnetic samples

Paired Samples (DCZ)	Depth (Meters)	Average of Paired Samples cgs (“volume”)
001/002	0.2286	0.0000239
003/004	1.2954	0.000019225
005/006	1.46304	0.00002205
007/008	2.3622	0.000006855
009/010	2.8956	0.000029125
011/012	4.4196	0.000012
013/014	6.3246	0.000006365
015/016	9.144	0.000026
017/018	10.5156	0.000047725
019/020	12.954	0.000018875
021/022	13.716	0.000012275
023/024	16.6116	1.14375E-05
025/026	18.7452	0.00000376
027/028	19.5072	0.00000632

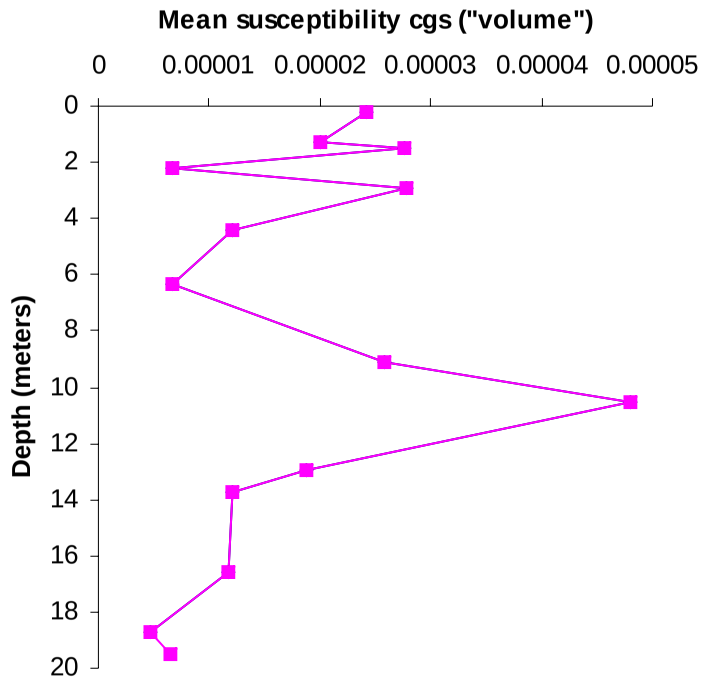

Table 2

Interpretation of paleomagnetic sampling results

Sample Number	Polarity	Interpretation	Comment
DCZ001	N	N	Normal
DCZ002	N		Normal
DCZ003	R	R?	South and down
DCZ004	R		South and up
DCZ005	R	R	Reversed
DCZ006	R		Reversed
DCZ007	R	R	Reversed
DCZ008	R		Reversed
DCZ009	R	R	Reversed
DCZ010	R		Reversed
DCZ011	R	R	Reversed
DCZ012	R		Reversed
DCZ013	R	R	Reversed
DCZ014	R		Reversed
DCZ015	N	N	Normal
DCZ016	N		Normal with a reversed VRM
DCZ017	N	N	Normal
DCZ018	N		Normal
DCZ019	N	N?	Beyond Origin
DCZ020	N		Beyond Origin
DCZ021	R	R	Reversed
DCZ022	R		Reversed
DCZ023	R	R?	South and down
DCZ024	R		South and down
DCZ025	R	R	Questionable Reversal
DCZ026	R		Reversed
DCZ027	R	R?	South and down
DCZ028	R		South and flat

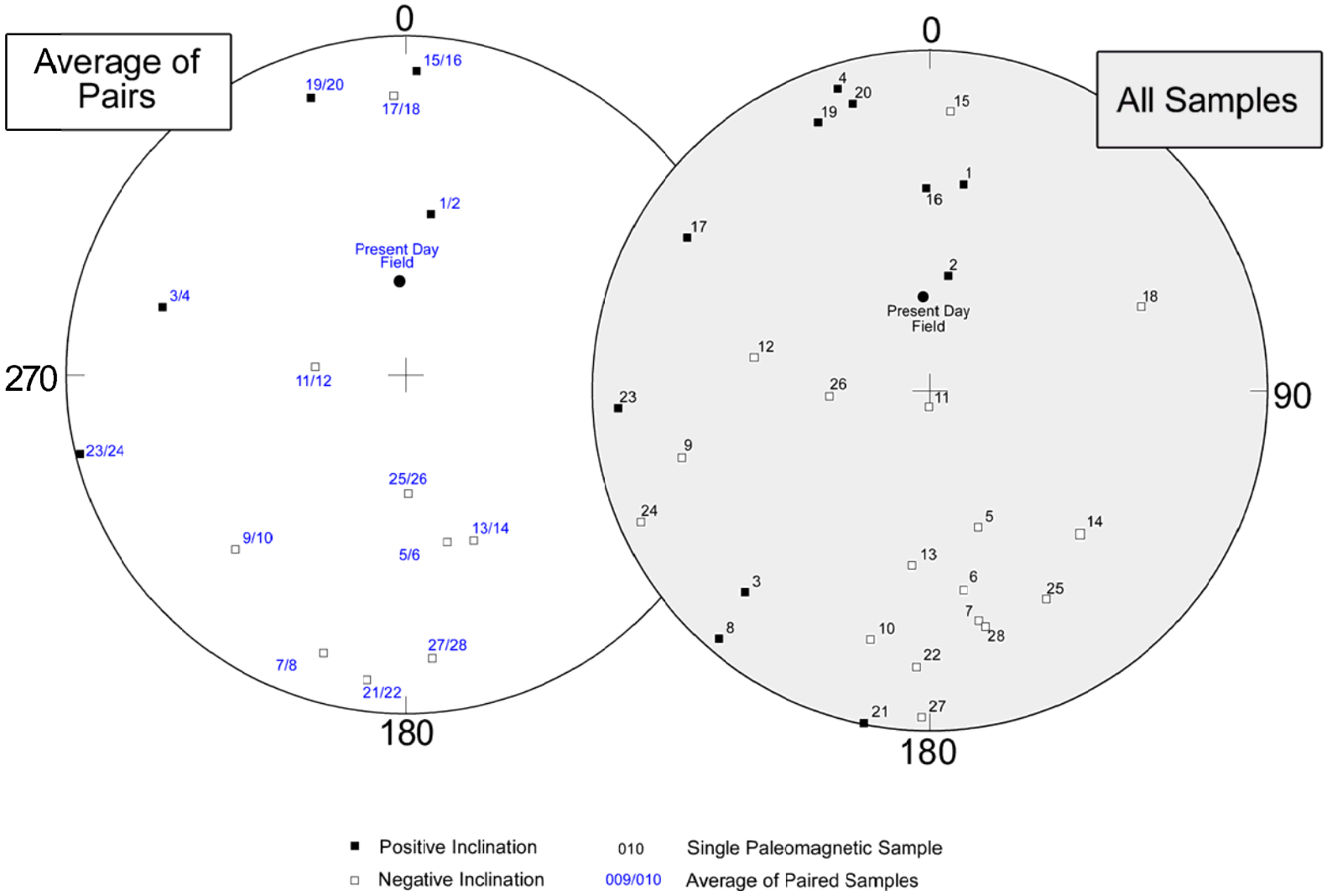

Figure 21. Schmidt equal area pole plots of characteristic remnant directions from paleomagnetic samples. All samples are from DCZ sample series.

of 0.780 to 0.990 million years. The next normal chron (C1r.1n) is represented in samples DCZ017 through DCZ020 at an age of 0.990 to 1.070 million years. The bottom most samples, DCZ026 through DCZ028, can be correlated to the preceding reversed chron (C1r.2r) at an age of 1.070 to 1.770 million years old. Therefore, the analysis of samples indicates that the minimum age of the cave is 1.070 million years old (Figure 22).

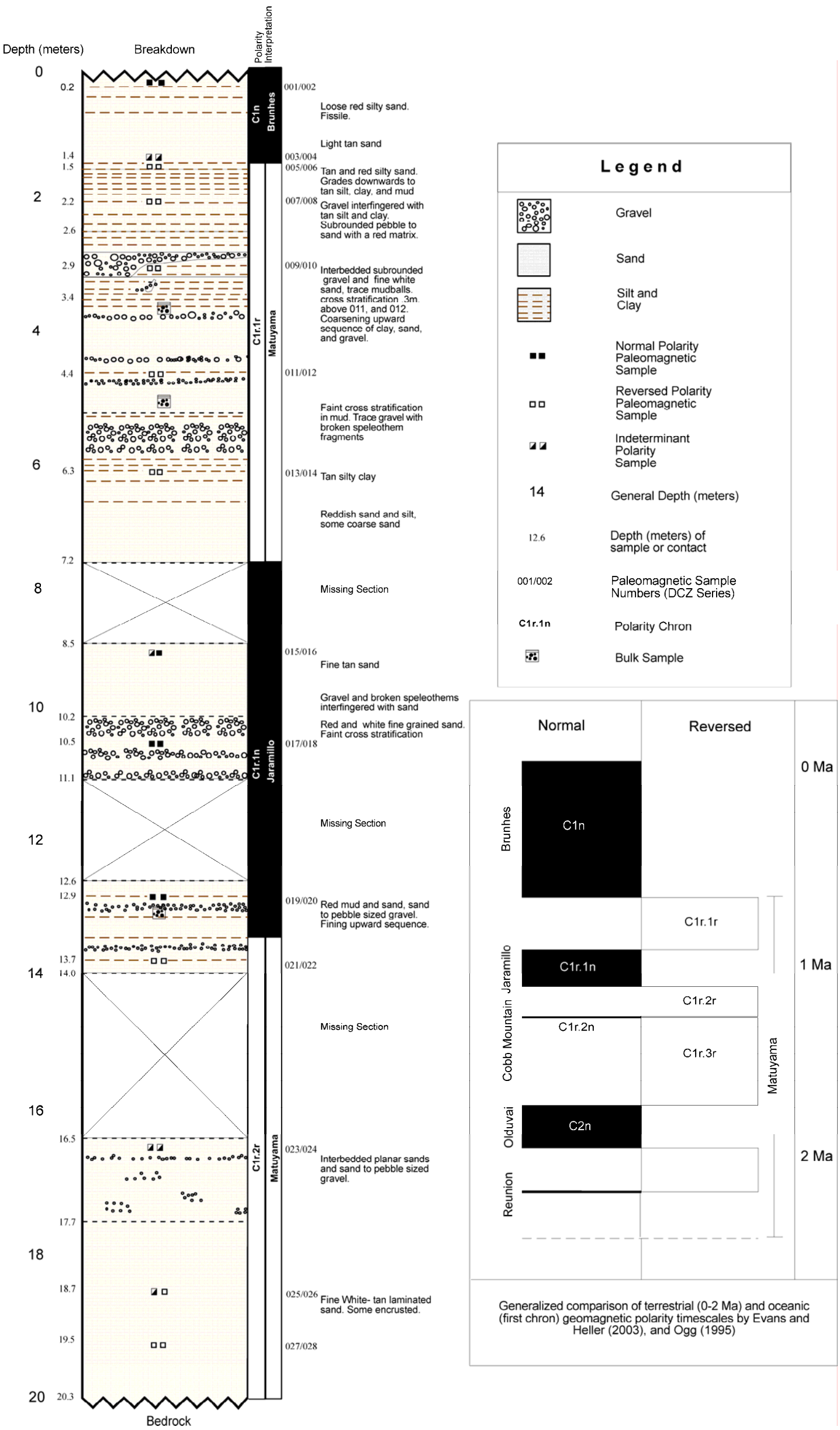

Figure 22. Stratigraphic column of Sand Hill showing paleomagnetic sediment sequence compared to geomagnetic polarity timescale.

CHAPTER V

PALEOHYDROLOGICAL INVESTIGATION

Introduction

In order to decipher the hydrologic origin of the cave, a paleohydraulic investigation was undertaken. All limestone caves form by flowing water. Direction, quantity, and source of paleo-water are useful to consider because they provide information on the initial cave-making environment. However, there is little flowing water in the presently known portion of Hellhole. Indications of paleoflow can be found in depositional structures, such as crossbeds, or erosional features such as scallops. Scallops are small dissolution features developed on bedrock walls. The limited occurrence of sediments in the cave required an emphasis on scallop measurements for determining paleoflow.

Scallops are formed by turbulent flow of a solvent over a soluble surface (Curl, 1974). They can be used to determine paleoflow direction and velocity of the karst waters. With this data, discharge can be calculated by taking velocity multiplied by the conduit diameter.

There are several challenges involved in this type of study. These include finding the remaining evidence, distinguishing between actual scallops and features that appear to be scallops, and determining flow direction from poor quality scallops. The

only evidence left is the actual scallops. They reveal the conditions at the last stages of when the conduit had flowing water. Scallops on breakdown walls can be lost or may be inverted from collapse.

It is difficult to quantify velocity and discharge of earlier stages of development due to the fact that conduits begin small and grow outward by dissolution. The scallops that represent the initial flow are dissolved and removed as the cave grows. In some locations scallops can show flow in opposing directions. This may be a result of flow reversals in the cave, or of local flow variability (eddies). A flow reversal may be the result of a flooding event that changes flow patterns surficially or in the subsurface by removing or depositing material.

Methods

The cave was traversed and scallops were located and measured. Four trips, totaling approximately 100 hours, were taken for the primary purpose of locating paleohydraulic indicators. In addition, scallops were sought on another 18 survey trips, which were taken for locating geologic and hydrologic data. Orientation and length of scallops was recorded using a compass and tape measure. On scallops that could be observed only from a distance, lengths were estimated. Also, meander scars were noted (to be used as supporting evidence of flow direction).

The paleohydraulic data was entered in to an Excel spreadsheet. With this database, calculations were made to determine flow velocity. Velocities were calculated

using an equation for deducing flow velocity from scallops (Curl, 1974). Table 3 defines the variables.

$$V = \frac{\mathrm{Re} \times \eta}{L \times \rho}$$

$$\mathrm{Re} = \mathrm{Re}^{\circ}\left[2.5\left(\ln\frac{D}{2L} - 1.5\right) + Bl\right]$$

Passage cross-sectional area was calculated by multiplying the average of the left and right and the average of the up and down of cave survey data at a survey station, then multiplying by pi. Discharge was then calculated by multiplying the paleo velocity by the cross-sectional area of the conduit. The result was then multiplied by two-thirds (assuming the passage was two-thirds full of water when scallops were forming). Later the cave was grouped into sections and the discharges of the grouped sections were averaged.

Results

Two hundred seventy five scallop measurements were recorded from 70 locations (Appendix F). From these measurements, 70 velocities and discharges were calculated.

Based upon the morphology of the cave, paleoflow direction can be discussed most easily by evaluating the cave as four sections. The four sections are the Northern extension, the Historical section, Bob's Big Break Borehole section, and the Southwest extension (Figure 23). Each one of these sections has characteristics different from the

Table 3

Explanation of variables from Curl's flow velocity equation

Symbol	Explanation
V	average velocity
L	scallop length (measured)
ρ	water density (0.998g/cm^3)
η	water viscosity (.0131g/cm)
Re	Reynolds number (calculated)
Re°	2200 (experimentally calculated)
D	Passage diameter (derived from cave survey data) – Sum of left and right from survey station
Bl	9.4 (experimentally calculated constant)

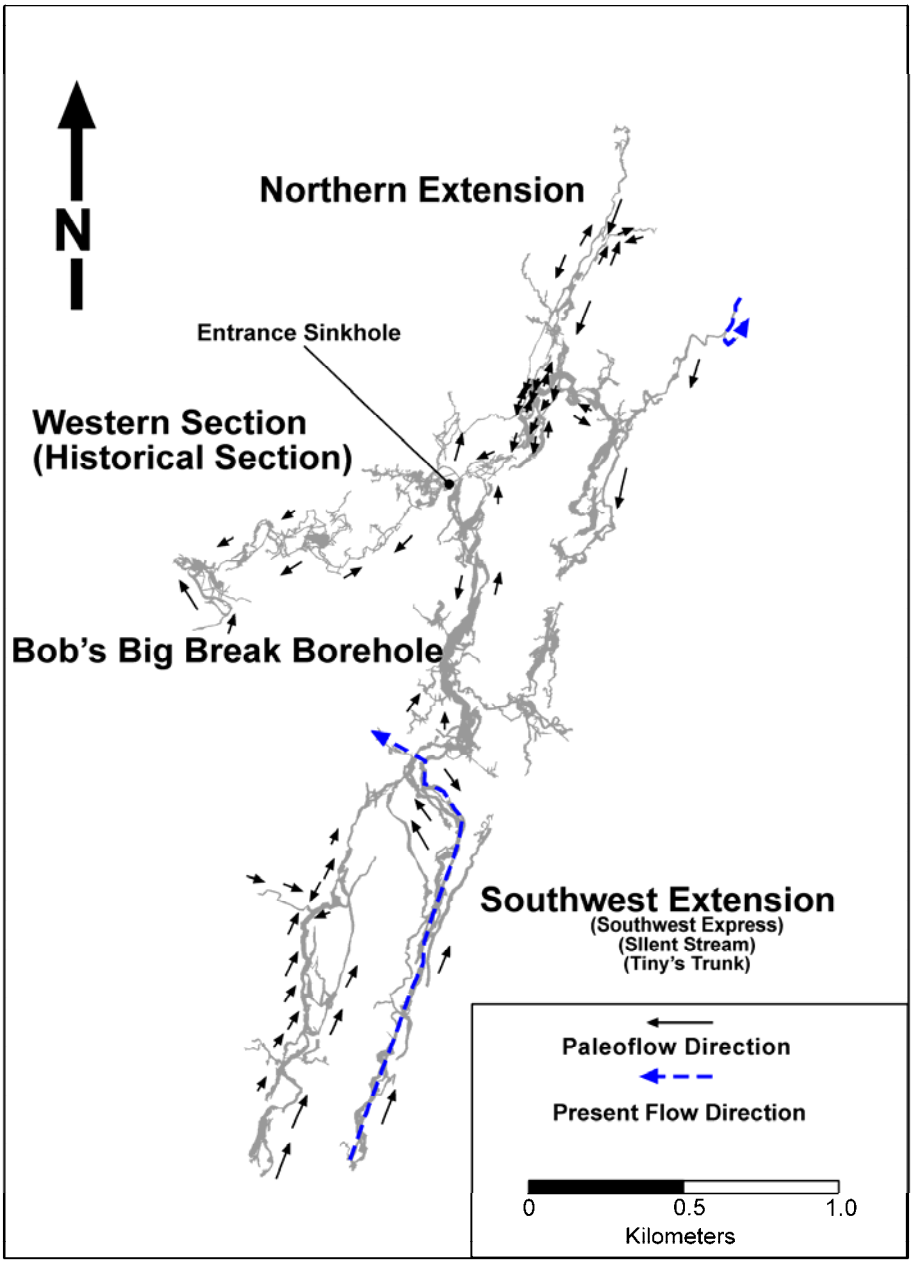

Figure 23. Map of paleoflow directions indicated by scallops in Hellhole.

others, and the overall cave morphology suggests possible different sources for waters.

The Northern extension consists mainly of secondary conduits of the branchwork pattern. Also, in some locations in the northern areas, a network type of passage was observed. 143 scallop measurements were located. Flow directions varied, and the average calculated discharge was 1.0 m^3/s. Some present day flow can be observed in the northeast corner of the Northern section.

In the Western section flow direction was primarily to the southwest with an average discharge of 1.1 m^3/s. The bulk of the Western section can be characterized as a series of very large rooms full of large breakdown blocks that form a complex maze of passages between the breakdown blocks. From the 18 paleohydraulic indications of scallops, the Western section may have been the primary path of karst waters to the discharge outlet of Judy Springs.

Bob's Big Break Borehole section can be described as the primary artery of the groundwater flow for a branchwork type system. The section is composed of large, relatively horizontal, passage with breakdown floors and ceilings. Due to the amount of breakdown from the walls and ceiling, paleoflow evidence is sparse and the paleoflow indication that was observed shows both northern and southern flow. More scallops quantitatively and prominently indicate southern flow. However, less prominent scallops as well as crossbedding in the sediments indicate northern flow.

In the Southwest extension, 113 scallops were located. The majority of evidence indicates flow heading North with an average discharge of 0.94 m^3/s. The passages that compose the Southern extension are the branchwork type secondary conduits that

intersect the primary artery of Bob's Big Break Borehole (Figure 24 and Figure 25). The majority of present day flow is observed in this area. The paleoflow directions mirror the present day flow in this section.

Figure 24. Photograph of a side passage of the Southwest Extension with scallops indicating flow out the page.

Figure 25. Photograph showing wall and ceiling scallops in a side passage of the Southwest Extension indicating flow into the page.

CHAPTER VI

DISCUSSIONS AND CONCLUSIONS

Discussion

In this investigation, several of the structural and hydraulic factors that influenced cavern development have been determined. In addition, a minimum age has been determined for Hellhole.

Based upon the strike data collected during this investigation, Germany Valley bedrock has a general primary strike direction of N25ºE to N30ºE. Variability in strike direction is due to the fact that the subsurface of the valley is highly deformed, as indicated by the observed faults within the cave. The presence of the structural deformation observed is directly related to the nearby Wills Mountain Anticline. Frequency of fracturing increases near the axis of an anticline (Davies, 1960).

The entrance sinkhole lies in a streambed between two small hills (Figure 26). The entrance sinkhole is in a present day streambed that is normally dry. Water can be witnessed flowing in to the cave via the entrance only during heavy rains. The abandoned stream channel continues to the West beyond the entrance sinkhole.

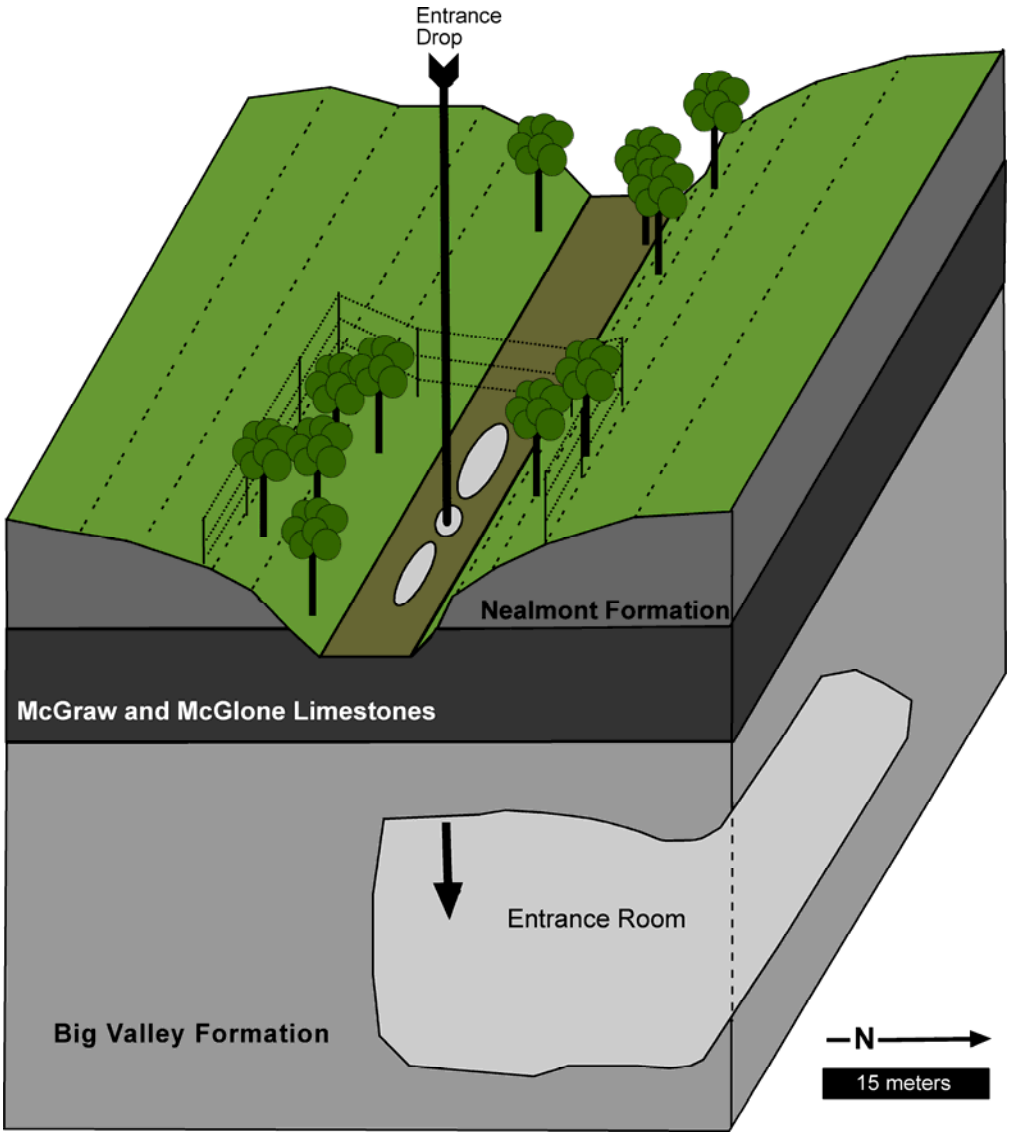

Figure 26. Schematic diagram of the entrance sink to Hellhole. Geology based upon visual observations. Dip of units is not shown, for sake of clarity.

The reason that the sinkhole developed at this location is related to the bedrock geology. The lithology at the crest of the sinkhole is the Nealmont Formation. The Nealmont Formation is a limestone that weathers easily in to a slope. The underlying units are the McGraw and McGlone Formations. The McGraw and McGlone are limestones that are more resistant ledge formers. The contact between the Nealmont and the McGraw and McGlone Formations is approximately 15 meters below the top of the sink. Surface waters initially ran through the streambed and eroded through the Nealmont and into the McGraw and McGlone Formations.

On the southern wall of the entrance drop about 25 meters from the top, the cylindrical shape of a vertical shaft was observed. The process that creates the cylindrical shape can only be formed by under saturated water flowing vertically downward in a void space under the influence of gravity (White, 2000). The feature is evidence that the connection from the surface to the cave was from surface waters, not from the genesis of the cave.

The entrance room itself has three passages leading out of it, one north, one south, and one west. The size of the room, and the fact that three passages intersect there with conflicting paleohydraulic evidence indicates that karst waters intersected in the entrance room (Figure 27).

From a spatial perspective, the highest passages (closest to the surface) are on the western side of the cave. These passages are “dry” with little to no active water. However, the passages on the eastern side are lower (further from the surface), and

Figure 27. Entrance to Hellhole

contain the active present day flow observed in the cave. Based upon the rose diagrams of cave passage frequency and strike data collected, cave passages parallel the bedrock strike (Figure 28). Since primary conduit development was influenced by bedrock strike and the fact that the dip of the bedrock in this area is to the east, the cave developed along strike, and then migrated down dip. The oldest passages are to the West; the youngest passages are to the East. Older passages are higher in elevation; younger passages are lower in elevation.

The Southern extension of the cave drains northward, the Northern extension indicates variability in flow directions, and the Western (Historic) section flows west. Bob's Big Break Borehole section also shows variability of flow with respect to scallop indication, but during the paleomagnetic investigation, cross bedding and the angle of sediment deposition indicates a northward flow direction that corresponds with the conduits to the South (Southern extension). The average discharges of the Northern, Southern, and Historical section are 1 m^3/s.

The unconsolidated sedimentary beds at the paleomagnetic sampling location (Sand Hill) have a strike of S32ºE degrees and a dip of 22ºSW. The beds were deposited in this orientation, because the size, position, and boundaries of the deposit are such that it would be impossible for them to be tilted en masse after deposition. The most reasonable explanation is that the passage became constricted. Water flow varied but sedimentary evidence reveals that at times, flow was rapid enough to carry material ranging from silts to gravel and remnants of broken speleothems. In one location rounded balls of mud were discovered. The sediment traveled in to the passage to where

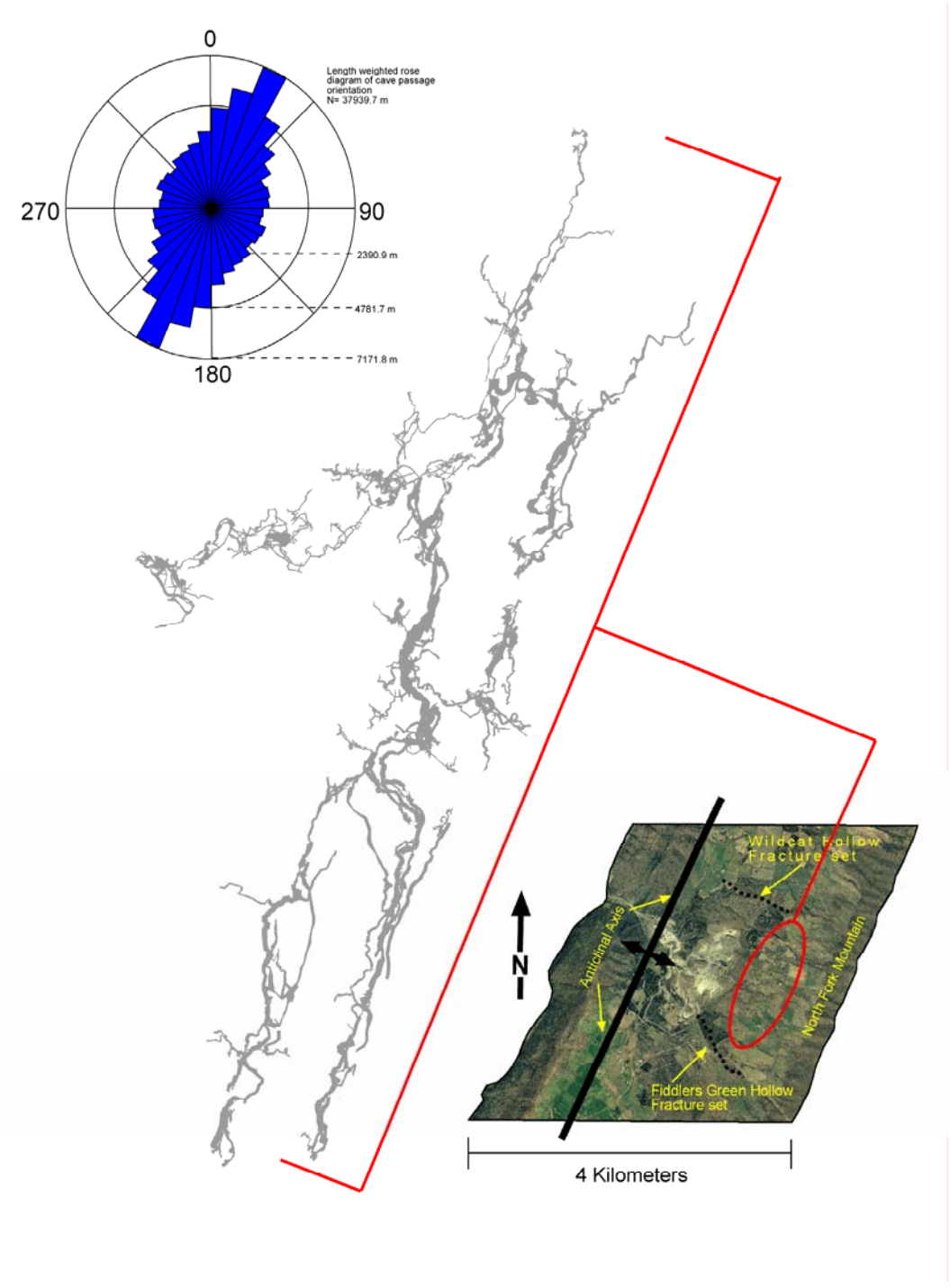

Figure 28. Comparison of Hellhole, cave passage rose diagram, and the Wills Mountain anticline

it encountered the constriction and the velocity slowed. The constriction that caused the reduction in velocity is no longer present. It is likely that breakdown created a dam that was the cause of the occluded flow. The sudden decrease in velocity resulted in the release of the sediment load as it traveled up gradient, forming the deposit on an angle. The passage was eventually abandoned preserving the sedimentary deposit. It was possible that the flow was phreatic. A vertical shaft began to develop over the passage. As the dome developed it intersected the cave at three levels, an upper level, the level containing the abandoned passage, and the lower passage. The constriction was eventually eroded away and the sediment deposit was exposed (Figure 29).

Although the sediment sand component was not quantified, it was observed that the sediments had a large sand fraction. Most other large West Virginia caves, such as Windy Mouth and Scott Hollow Cave (Monroe and Greenbrier Counties), have predominantly silt and clay sediments. In addition, these caves also contain a lot of chert in the sediment due to the nature of the bedrock (Curry, 2003; Haney, 2002). Germany Valley is however, surrounded by three sandstone units. The high sand constituent is most likely a result of the surficial weathering of these sandstone caprocks.

During the course of this investigation it was noted that the water table was encountered in the cave at depths of approximately 130 meters (GVKS survey). However, the local residents have domestic water wells much higher than the (cave) water table. Other Germany Valley residents have wells that penetrate to the cave depth water table. This is evaluated in the following paragraph.

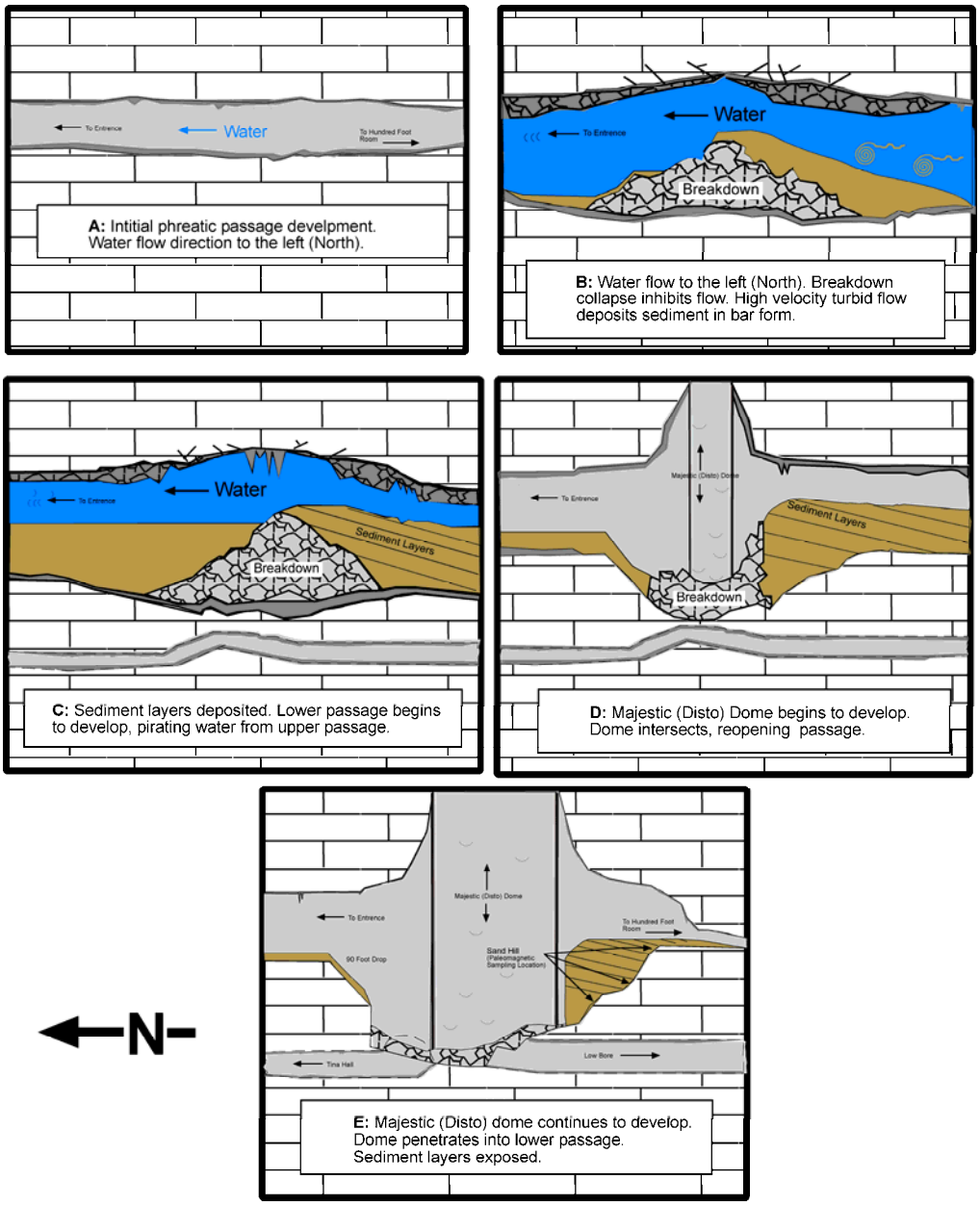

Figure 29. Schematic diagram of the origin of the Sand Hill region of Hellhole

The local mountain surface drainage is penetrating the surface and stored in an upper aquifer, above Hellhole (Figure 30). Evidence of this upper aquifer is the presence of the domestic water wells above the cave and presence of surface springs above Hellhole. A lower aquifer includes Hellhole. The properties of the confining unit between the upper and lower aquifers are unknown. The elevations of the bottom of the well in the central valley (506 meters) and water encountered in the cave (530 meters) are nearly the same as Judy Spring (537 meters) and the North Fork of the Potomac River (518 meters). Due to the similarity in elevation of the water encountered in the cave and that of the North Fork River and Judy Springs, the groundwater flowing through the cave does represent regional base level. In addition, the majority of the current groundwater flow in the cave and the paleoflow indicated from the entrance to the south is the same direction (North) as the North Fork River.

The minimum age of the sediments from Sand Hill was determined to be 1.070 million years. The magnetostratigraphic column presented is the most complete yet found in the Appalachian Mountains. The age also implies that the cave began forming during the Pleistocene. During the glacial/interglacial sequences of the Pleistocene, variability in sea level and potentiometric surfaces occurred. Climate changes that occurred during the interglacial periods are a possible explanation to changing environments and thus a potential source of water to produce the velocities and the discharges calculated from the paleohydraulic investigation.

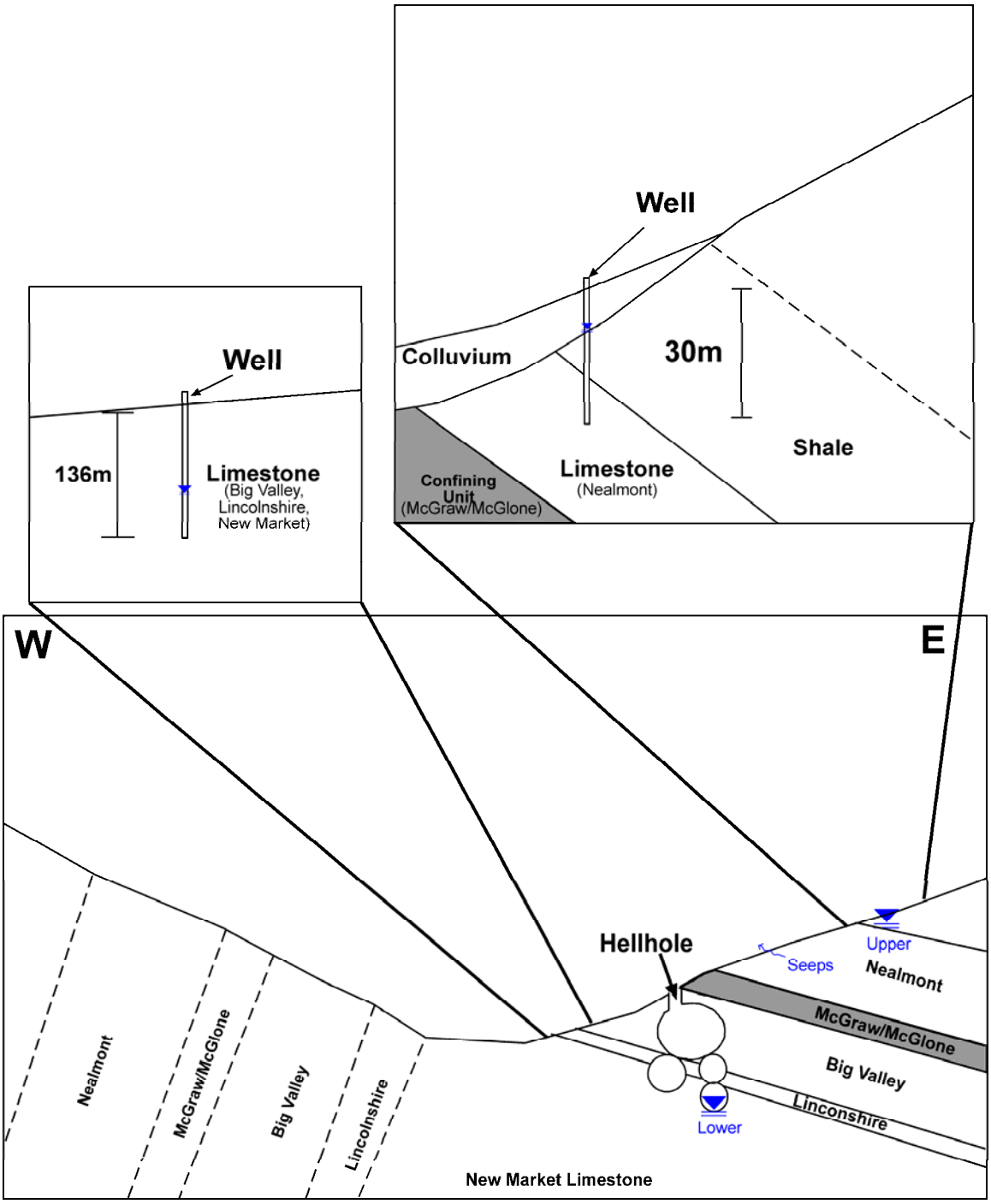

Figure 30. Schematic diagram of relationship of upper and lower aquifers present in Germany Valley.

This study has been inconclusive as to a source of groundwater for cavern development in this area. The facts are that cave base level (valley-wide) is equivalent to the level of the North Fork River level and that other nearby caves (Memorial Day Cave, Shovel Eater Cave) exist and have similar trends (i.e. large North-South passages that run parallel to strike). Exploration and survey of Germany Valley caves is ongoing. If the three caves were connected, there would be potential for a 65-kilometer cave system to exist in the subsurface of this valley.

Conclusions

Every known area of Hellhole was visited and analyzed with respect to structural features and paleohydraulic indicators. A paleomagnetic sampling location was chosen and sampled. This investigation evaluated the following three hypotheses, which are reiterated below along with the pertinent findings.

1. The borehole passage of Hellhole was formed as a result of mountain surface drainage sinking, and then flowing parallel to bedrock strike. Mountain surface drainage influenced the formation of the cave, but the data are inconclusive as to the quantity of the significance of the influence. Sand deposited in the cave is likely derived from erosion of ridge-capping sandstone. Based upon the passage development primarily being influenced by the strike of the valley, depths and spatial orientation of levels of the cave, and locations of the present day groundwater flow in the cave, the cave developed along strike and down dip.

2. The entrance sinkhole resulted from the confluence of several underground streams. Based upon the paleohydraulic data, the entrance room was an intersection of

several underground streams. However, the connection from the room to the surface is more shaft-like from surface water penetration. It is unlikely that the confluence of streams formed the entrance. It is more likely that a preferential joint existed that was enlarged from incoming surface waters to connect both the surface and the subsurface cavity. In other words, the present day entrance is more a result of surface erosion than a major genetic feature of the cave.

3. Horizontal passage development in Hellhole Cave is a result of water flowing along strike to the discharge area of Judy Springs. The variability in the strikes collected during this investigation gives evidence of the abundance of the amount of structural deformation present in the valley. The rose diagram of the frequency of cave passage shows the greatest amount of passage in the same direction as the primary strike of the valley, approximately 25 to 30 degrees. Therefore, the primary passage development was controlled by groundwater flowing along the primary strike of the valley, and not influenced by perpendicular structural deformation. Hellhole has not been dye-traced. However, nearby Schoolhouse Cave has been dye-traced to Judy Spring (Brace, 2003). Based upon the close proximity of the caves, and the proximity to Judy Spring, it is likely that Hellhole also discharges to Judy Springs. In addition, the structure of the conduit system, paleohydraulic evidence, and the most prominent present day hydraulic flow (Southern extension) supports the hypothesis. However, in order for water to discharge to Judy Spring, water has to flow across dip. The course is unclear but must be related to the structure of the nearby Wills Mountain anticline.

REFERENCES

Brace, G., 2000, Geology of Germany Valley, Pendleton County, West Virginia (Map) Privately Published.

Brace, G., 2003 personal conversation.

Cande, S.C., and Kent, D.V., 1995, Revised calibration of the geomagnetic polarity timescale for the Late Cretaceous and Cenozoic: Journal of Geophysical Research, v. 100, no. B4, p. 6093-6095.

Chapman, M.E., 1970, Pendleton County's saltpeter caves and their role in the Civil War: Speleo Digest, p. 308-309.

Curl, R.L., 1974, Deducing flow velocity in cave conduits from scallops: National Speleological Society Bulletin, v. 36, no. 2, p. 1-5.

Curry, M., 2003, Sediments from an abandoned karst groundwater conduit: Windy Mouth Cave, Greenbrier County, West Virginia: Undergraduate Study, University of Akron, 26 p.

Culver, D.C., and White, W.W., 2005, Encyclopedia of Caves: Elsevier, p. 427-430.

Dasher, G., 2000, The caves of east-central West Virginia: West Virginia Speleological Survey Bulletin # 14, 182.

Dasher, G., 2001, The caves and karst of Pendleton County: West Virginia Speleological Survey Bulletin #15, p. 17-42, 200-203, 290.

Davies, W.E., 1960, Origin of caves in folded limestone: National Speleological Society Bulletin, v. 22, no.1, p. 5-18.

Deike, R. G., 1969, Relations of jointing to orientation of solutional cavities in limestones of central Pennsylvania: American Journal of Science, v. 267, p. 1230-1248.

Drabbish, R.A., and Sites, R.S., 1982, The structural development and deformation of the Allegheny frontal zone and the Wills Mountain Anticlinorium. The Central Eastern Overthrust Belt: Appalachian Geological Society field trip guidebook, 50th anniversary edition, 106 p.

Edwards, J., 1959, Germany Valley Speleological Report: Speleodigest No.2, p. 55-69.

Evans, M.E. and Heller, F., 2003, Environmental Magnetism: Principles and applications of enviromagnetics: Academic Press, p. 118-143.

Ford, D.C., and Williams, P.W., 1989, Karst geomorphology and hydrology: London, Unwin Hyman, 601 p.

Fountainware, 2003, COMPASS software, http://www.fountainware.com/compass/

Germany Valley Karst Survey (GVKS), 2004 Hellhole Survey Data: Compass File Private availability.

Gunn, J., 2004 (ed.), Paleoenvironments: Clastic cave sediments: in Culver, D.C., and White, W.B., Encyclopedia of Caves and Karst Science: Taylor and Francis Books, New York, NY., p. 553-555.

Haney, S., 2002, A study of Scott Hollow Cave: Sediment provenance, magnetic properties and deposition of sediment in the tourist area of Scott Hollow Cave: Undergraduate Study, University of Akron, 26 p.

Jones, W.K., 1997, Karst hydrology atlas of West Virginia: Karst Waters Institute Special Publication 4, Charles Town, West Virginia, 111 p.

Kisamore, Daniel, 2005, personal conversation.

Kulander, B.R., and Dean, S.L., 1986, Structure and tectonics of Central and Southern Appalachian Valley and Ridge Plateau Provinces, West Virginia and Virginia: American Association of Petroleum Geologists Bulletin, v. 70, no. 11, p. 1674-1684.

McColloch, J.S., 1986, Springs of West Virginia: 50th anniversary revised edition: West Virginia Geological and Economic Survey, v. V-6A, 493p.

Ogg, J.G., 1995, Magnetic polarity time scale of the Phanerozoic: Global Earth Physics, p. 240-270.

Palmer, A.N., 1975, The origin of maze caves: National Speleological Society Bulletin, v. 37, p. 57-76.

Palmer, A.N., 1991, Origin and morphology of limestone caves: Geological Society of America Bulletin, v. 103, p. 1-21.

Parizek, R.R., White, W.B., and Langmuir, D., 1971, Hydrology and geochemistry of folded and faulted rocks of the central Appalachian type and related land use problems: The Pennsylvania State University, Earth and Mineral Sciences Experiment Station – Mineral Conservation Series Circular 82, 212 p.

Perry, W., J. 1975, Tectonics of the Western Valley and Ridge Foldbelt, Pendleton County, West Virginia: Journal of Research of U.S. Geologic Survey, v. 3, no. 5, p. 583-588

Rockware, 2002, GeoTrig software, http//www.rockware.com/catalog/free.html

Sasowsky, I.D., White, W.B., and Schmidt, V.A., 1995, Determination of stream-incision rate in the Appalachian Plateaus by using cave-sediment magnetostratigraphy: Geology, v. 23, no. 5, p. 415-418.

Schmidt, V.A., 1982, Magnetostratigraphy of sediments in Mammoth Cave, Kentucky: Science, v. 217, p. 827-829.

Sites, R., 1971, Geology of the Smoke Hole region in Grant and Pendleton Counties, West Virginia: Master of Science Thesis, West Virginia University, 103 p.

West Virginia GIS Technical Center, 2003, http://wvgis.wvu.edu/data/dataset

White, W.B., 1988, Geomorphology and hydrology of karst terrains: Oxford University Press, p. 96-99.

White W.B., 2000, Speleogenesis of vertical shafts in the Eastern United States: in Klimchoulk, A.B., Ford, D.C., Palmer, A.N., and Dreybolt, W., Speleogenesis: Evolution of karst aquifers: National Speleological Society Huntsville, Alabama, p. 378-381.

Wilson, F., 1977, Judy Spring, Pendleton County, West Virginia: Speleo Digest, p. 85-86.

Zidjerveld, J.D. A., 1967, A. C. demagnetization of rocks: Analysis of results, in Collinsion, D. W., Creer, K.M., and Runcorn, S.K., (eds.) Methods in paleomagnetism: Amsterdam, Elsevier, p. 254-286.

APPENDICES

APPENDIX A

WEST VIRGINIA STATE DEPARTMENT OF HEALTH WELL COMPLETION REPORT

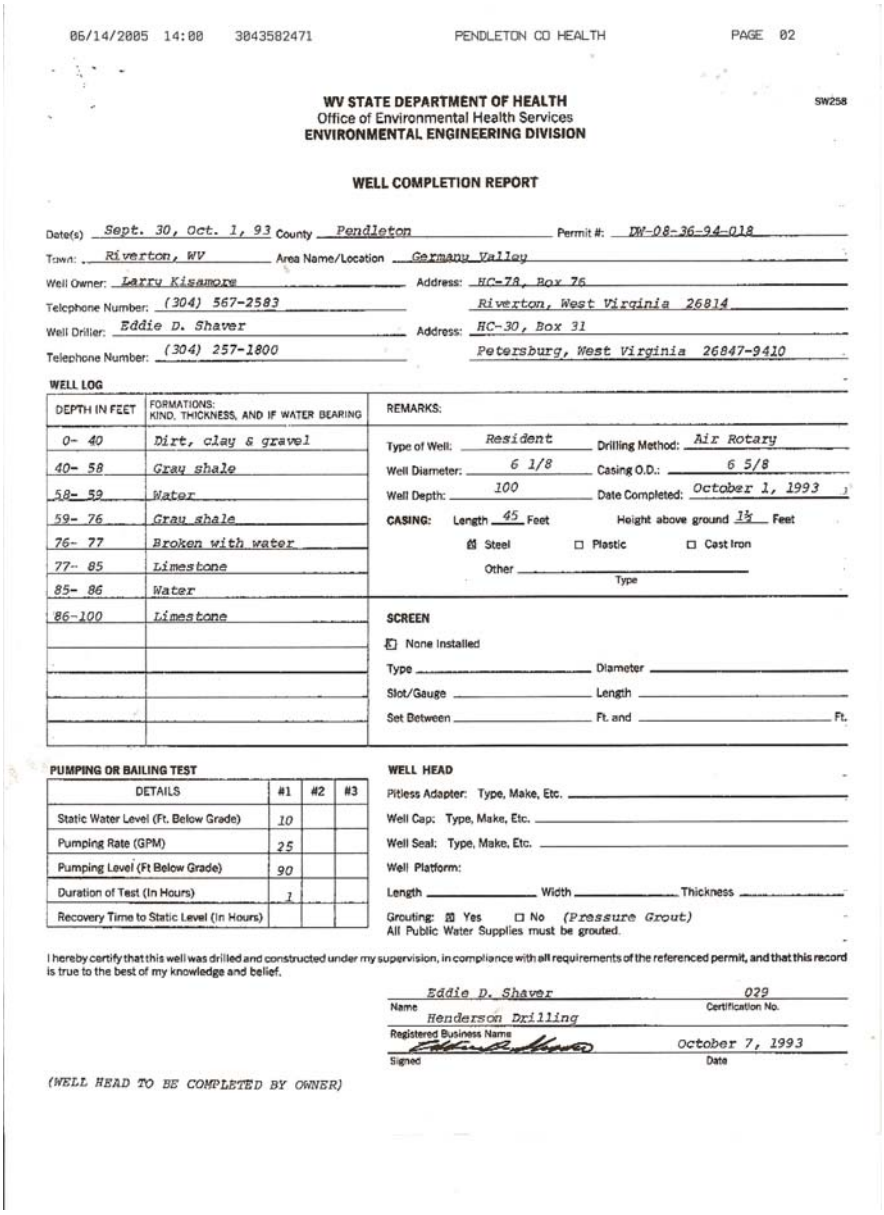

06/14/2005 14:00 3043582471 PENDLETON CO HEALTH PAGE 02

WV STATE DEPARTMENT OF HEALTH
Office of Environmental Health Services
ENVIRONMENTAL ENGINEERING DIVISION

SW258

WELL COMPLETION REPORT

Date(s) Sept. 30, Oct. 1, 93 County Pendleton Permit #: DW-08-36-94-018
Town: Riverton, WV Area Name/Location Germany Valley
Well Owner: Larry Kisamore Address: HC-78, Box 76
Telephone Number: (304) 567-2583 Riverton, West Virginia 26814
Well Driller: Eddie D. Shaver Address: HC-30, Box 31
Telephone Number: (304) 257-1800 Petersburg, West Virginia 26847-9410

WELL LOG

DEPTH IN FEET	FORMATIONS: KIND, THICKNESS, AND IF WATER BEARING
0- 40	Dirt, clay & gravel
40- 58	Gray shale
58- 59	Water
59- 76	Gray shale
76- 77	Broken with water
77- 85	Limestone
85- 86	Water
86-100	Limestone

REMARKS:

Type of Well: Resident Drilling Method: Air Rotary
Well Diameter: 6 1/8 Casing O.D.: 6 5/8
Well Depth: 100 Date Completed: October 1, 1993
CASING: Length 45 Feet Height above ground 1½ Feet
☒ Steel ☐ Plastic ☐ Cast Iron
Other ____ Type

SCREEN
☐ None Installed
Type ____ Diameter ____
Slot/Gauge ____ Length ____
Set Between ____ Ft. and ____ Ft.

PUMPING OR BAILING TEST

DETAILS	#1	#2	#3
Static Water Level (Ft. Below Grade)	10		
Pumping Rate (GPM)	25		
Pumping Level (Ft Below Grade)	90		
Duration of Test (In Hours)	1		
Recovery Time to Static Level (In Hours)			

WELL HEAD
Pitless Adapter: Type, Make, Etc. ____
Well Cap: Type, Make, Etc. ____
Well Seal: Type, Make, Etc. ____
Well Platform:
Length ____ Width ____ Thickness ____
Grouting: ☒ Yes ☐ No (Pressure Grout)
All Public Water Supplies must be grouted.

I hereby certify that this well was drilled and constructed under my supervision, in compliance with all requirements of the referenced permit, and that this record is true to the best of my knowledge and belief.

Eddie D. Shaver (Name) 029 (Certification No.)
Henderson Drilling (Registered Business Name)
Signed ____ October 7, 1993 (Date)

(WELL HEAD TO BE COMPLETED BY OWNER)

APPENDIX B

STRIKE AND DIP OF BEDDING PLANES AND FAULTS FROM WITHIN AND OVER HELLHOLE

Strike and Dip Measurements of Bedding Planes in Hellhole

Location (GVKS Survey)	Strike	Dip	Comment
HE24	N35W	--	--
LC23	N29E	19W	Good Surface
NF10	N85E	28W	--
Fault Room	N65E	8W	--

Strike and Dip Measurements of Observed Faults in Hellhole

Location (GVKS Survey)	Strike	Dip	Comment
DD104	N28E	16E	FAULT
DD68	N60W	9W	FAULT
DD68	N60W	16W	FAULT
Crystal Palace	N90E	78W	FAULT
HAQ 25	N5W	49E	Fractured Area
End of Crystal Palace	N45E	90	Vertical Bed
Rat 29	N28E	90	Vertical Bed
End of HSB	--	--	FAULT
Dartt Canyon	--	--	FAULT
AR 29	--	--	FAULT
Raccoon Passage	--	--	FAULT
Window Dome	--	--	FAULT

Strike and Dip Measurements above Hellhole			
Location	**Strike**	**Dip**	**Comment**
1	N26E	10E	
2	N90W	25W	
3	N70W	11W	

APPENDIX C

PALEOMAGNETIC SAMPLE ORIENTATION DATA

Abbreviation	Description	
Sample ID	Sample Number	
Quantity	Quantity (8cc cube)	
q	V	Measurement is by volume
c	S	Sample box strike & dip are recorded and bedding strike & dip are recorded
v	V	Sample lat/long given, so VGP may be calculated
r	R	The sample top is rotated (a Phi or other value is present)
LV	Local Variation	
SamAz	Sample Azimuth (sum of strike and 270° , calculated by the program)	
Samß	Sample Beta (for us, program calculates as -SmDip)	
SmStr	Strike of Sample Cube face (Brunton arm facing left)	
SmDip	Dip of Sample Cube	
BdStr	Strike of Sediment Horizon	
BdDip	Dip of Sediment Horizon	
Phi	Tilt (rotation) of Sample Cube	
SiteLt	Latitude of Study Area	
SiteLn	Longitude of Study Area	

Sample ID	Quant qcvr	LV	SamAz	Samß	SmStr	SmDip	BdStr	BdDip	Phi	SiteLt	SiteLn
DCZ001	8.00VSVR	-9.1	304	-68	34	68	148	22	5	38.77	-79.38
DCZ002	8.00VSVR	-9.1	329	-73	59	73	148	22	9	38.77	-79.38
DCZ003	8.00VSVR	-9.1	258	-62	348	62	148	22	15	38.77	-79.38
DCZ004	8.00VSVR	-9.1	257	-64	347	64	148	22	18	38.77	-79.38
DCZ005	8.00VSVR	-9.1	274	-71	4	71	148	22	3	38.77	-79.38
DCZ006	8.00VSVR	-9.1	275	-64	5	64	148	22	5	38.77	-79.38
DCZ007	8.00VSVR	-9.1	300	-84	30	84	148	22	6	38.77	-79.38
DCZ008	8.00VSVR	-9.1	302	-71	32	71	148	22	9	38.77	-79.38
DCZ009	8.00VSVR	-9.1	265	-74	355	74	148	22	3	38.77	-79.38
DCZ010	8.00VSVR	-9.1	257	-60	347	60	148	22	1	38.77	-79.38
DCZ011	8.00VSVR	-9.1	273	-64	3	64	148	22	-6	38.77	-79.38
DCZ012	8.00VSVR	-9.1	224	-52	314	52	148	22	-11	38.77	-79.38
DCZ013	8.00VSVR	-9.1	270	-70	360	70	148	22	3	38.77	-79.38
DCZ014	8.00VSVR	-9.1	261	-65	351	65	148	22	-9	38.77	-79.38
DCZ015	8.00VSVR	-9.1	258	-48	348	48	148	22	2	38.77	-79.38
DCZ016	8.00VSVR	-9.1	258	-46	348	46	148	22	6	38.77	-79.38
DCZ017	8.00VSVR	-9.1	216	-56	306	56	148	22	-15	38.77	-79.38
DCZ018	8.00VSVR	-9.1	222	-59	312	59	148	22	-11	38.77	-79.38
DCZ019	8.00VSVR	-9.1	273	-51	3	51	148	22	0	38.77	-79.38
DCZ020	8.00VSVR	-9.1	287	-51	17	51	148	22	6	38.77	-79.38
DCZ021	8.00VSVR	-9.1	16	-72	106	72	148	22	0	38.77	-79.38
DCZ022	8.00VSVR	-9.1	5	-64	95	64	148	22	0	38.77	-79.38
DCZ023	8.00VSVR	-9.1	319	-64	49	64	148	22	4	38.77	-79.38
DCZ024	8.00VSVR	-9.1	322	-71	52	71	148	22	4	38.77	-79.38
DCZ025	8.00VSVR	-9.1	277	-57	7	57	148	22	3	38.77	-79.38
DCZ026	8.00VSVR	-9.1	264	-64	354	64	148	22	2	38.77	-79.38
DCZ027	8.00VSVR	-9.1	221	-68	311	68	148	22	-7	38.77	-79.38
DCZ028	8.00VSVR	-9.1	234	-71	324	71	148	22	-5	38.77	-79.38

APPENDIX D

ZIJDERVELD DIAGRAMS

Numbers along lines are AF demagnetization levels in mT.

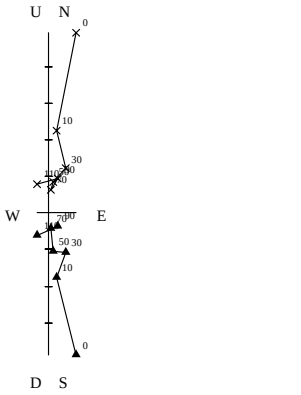

Horiz: ×
Vert: ▲

Tick interval = 10^{-6} KA m^{-1}

DCZ001 Geographic AF Demag

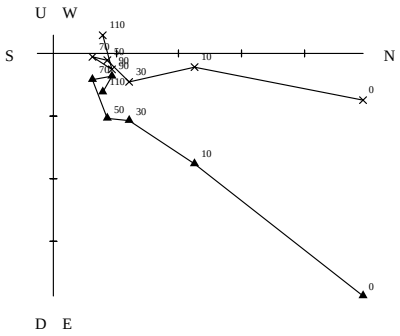

Horiz: ×
Vert: ▲

Tick interval = 10^{-6} KA m^{-1}

DCZ001 Geographic AF Demag

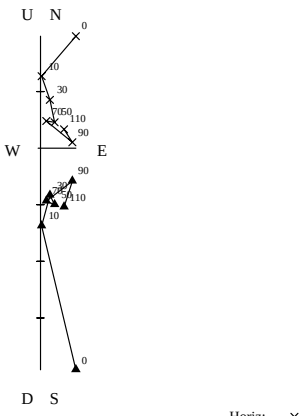

Horiz: ×
Vert: ▲

Tick interval = 10^{-6} KA m^{-1}

DCZ002 Geographic AF Demag

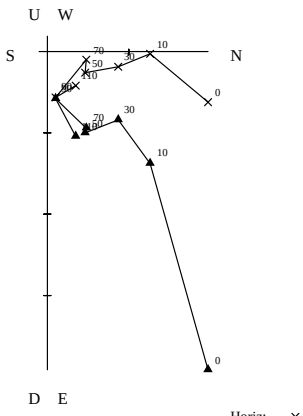

Horiz: ×
Vert: ▲

Tick interval = 10^{-6} KA m^{-1}

DCZ002 Geographic AF Demag

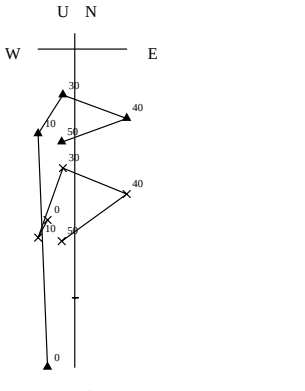

Horiz: ×
Vert: ▲

Tick interval = 10^{-6} KA m^{-1}

DCZ003 Geographic AF Demag

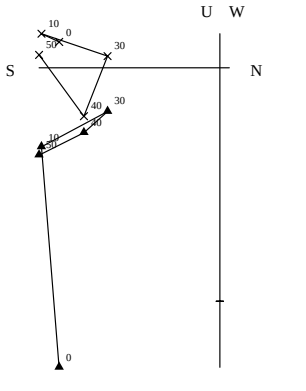

Horiz: ×
Vert: ▲

Tick interval = 10^{-6} KA m^{-1}

DCZ003 Geographic AF Demag

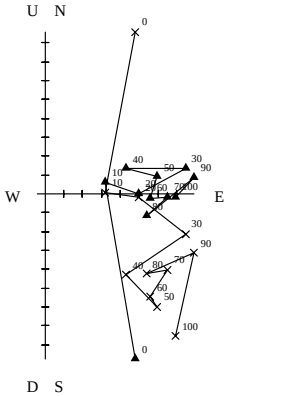

Horiz: ×
Vert: ▲

Tick interval = 10^{-7} KA m^{-1}

DCZ004 Geographic AF Demag

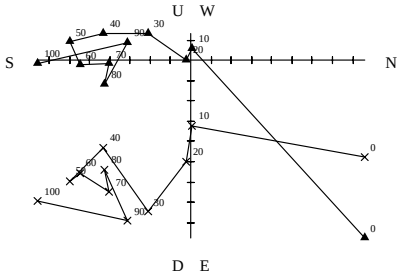

Horiz: ×
Vert: ▲

Tick interval = 10^{-7} KA m^{-1}

DCZ004 Geographic AF Demag

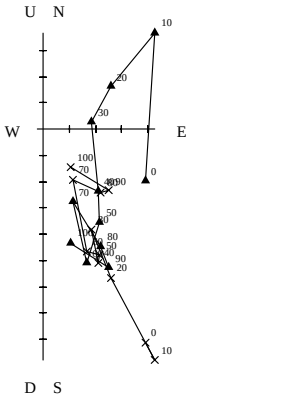

Horiz: ×
Vert: ▲

Tick interval = 10^{-7} KA m^{-1}

DCZ005 Geographic AF Demag

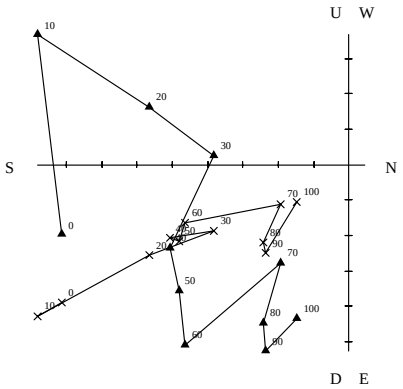

Horiz: ×
Vert: ▲

Tick interval = 10^{-7} KA m^{-1}

DCZ005 Geographic AF Demag

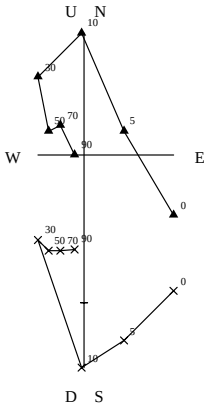

Horiz: ×
Vert: ▲

Tick interval = 10^{-6} KA m^{-1}

DCZ006 Geographic AF Demag

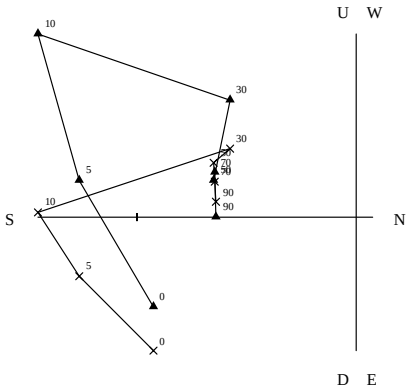

Horiz: ×
Vert: ▲

Tick interval = 10^{-6} KA m^{-1}

DCZ006 Geographic AF Demag

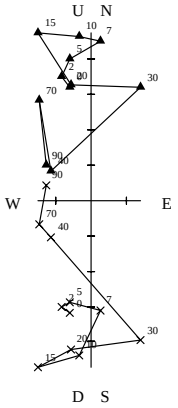

Horiz: ×
Vert: ▲

Tick interval = 10^{-7} KA m^{-1}

DCZ007 Geographic AF Demag

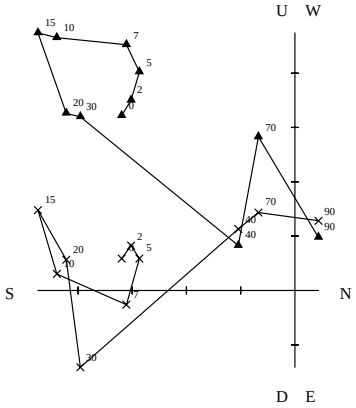

Horiz: ×
Vert: ▲

Tick interval = 10^{-7} KA m^{-1}

DCZ007 Geographic AF Demag

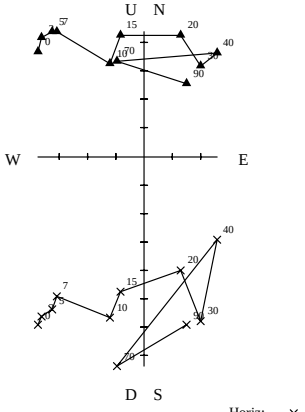

Tick interval = 10^{-7} KA m^{-1} Horiz: ×
Vert: ▲

DCZ008 Geographic AF Demag

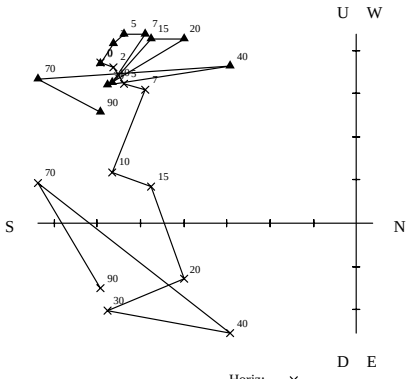

Tick interval = 10^{-7} KA m^{-1} Horiz: ×
Vert: ▲

DCZ008 Geographic AF Demag

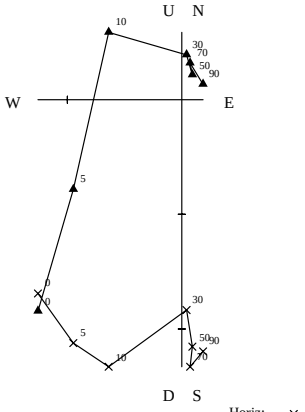

Tick interval = 10^{-6} KA m^{-1} Horiz: ×
Vert: ▲

DCZ009 Geographic AF Demag

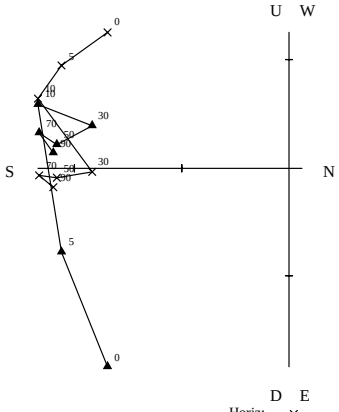

Tick interval = 10^{-6} KA m^{-1} Horiz: ×
Vert: ▲

DCZ009 Geographic AF Demag

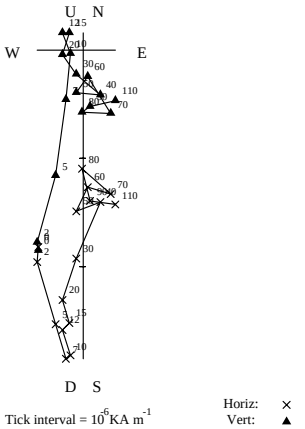

Tick interval = 10^{-6} KA m^{-1} Horiz: ×
Vert: ▲

DCZ010 Geographic AF Demag

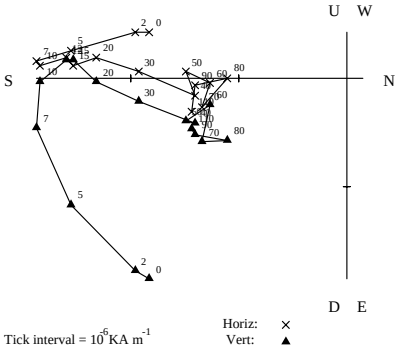

Tick interval = 10^{-6} KA m^{-1} Horiz: ×
Vert: ▲

DCZ010 Geographic AF Demag

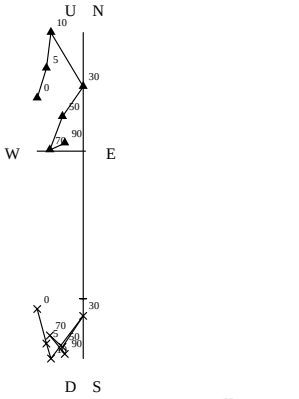

Horiz: ×
Tick interval = 10^{-6} KA m^{-1} Vert: ▲
DCZ011 Geographic AF Demag

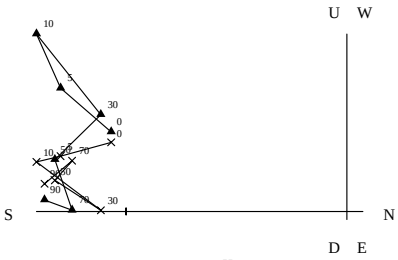

Horiz: ×
Tick interval = 10^{-6} KA m^{-1} Vert: ▲
DCZ011 Geographic AF Demag

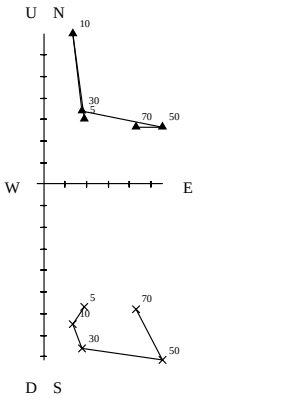

Horiz: ×
Tick interval = 10^{-7} KA m^{-1} Vert: ▲
DCZ012 Geographic AF Demag

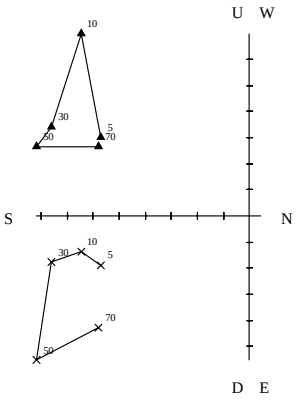

Horiz: ×
Tick interval = 10^{-7} KA m^{-1} Vert: ▲
DCZ012 Geographic AF Demag

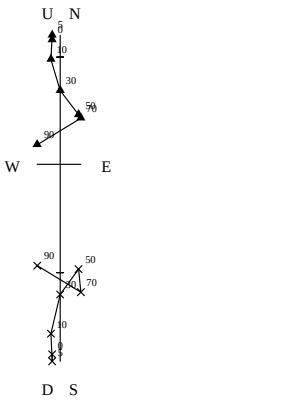

Horiz: ×
Tick interval = 10^{-6} KA m^{-1} Vert: ▲
DCZ013 Geographic AF Demag

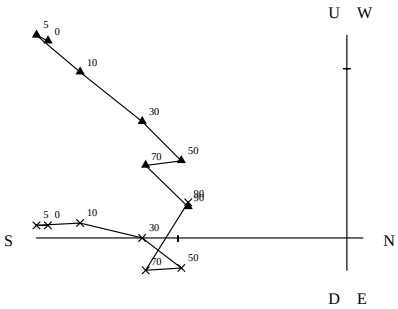

Horiz: ×
Tick interval = 10^{-6} KA m^{-1} Vert: ▲
DCZ013 Geographic AF Demag

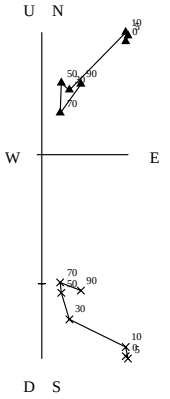

Horiz: ×
Tick interval = 10^{-6} KA m^{-1} Vert: ▲
DCZ014 Geographic AF Demag

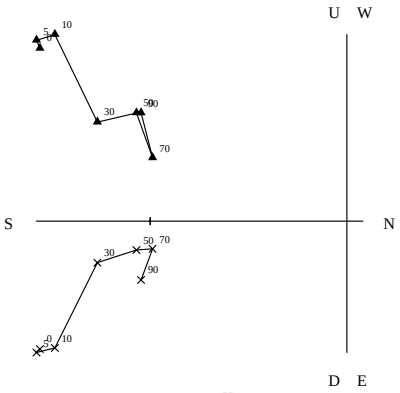

Horiz: ×
Tick interval = 10^{-6} KA m^{-1} Vert: ▲
DCZ014 Geographic AF Demag

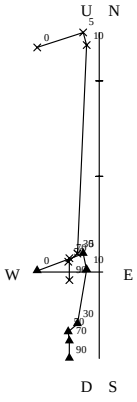

Horiz: ×
Tick interval = 10^{-6} KA m^{-1} Vert: ▲
DCZ015 Geographic AF Demag

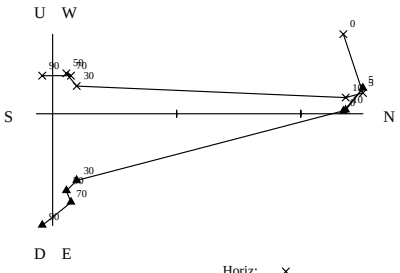

Horiz: ×
Tick interval = 10^{-6} KA m^{-1} Vert: ▲
DCZ015 Geographic AF Demag

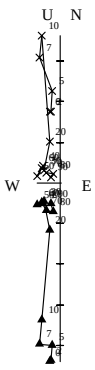

Horiz: ×
Tick interval = 10^{-6} KA m^{-1} Vert: ▲
DCZ016 Geographic AF Demag

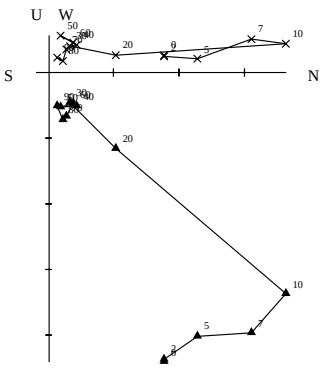

Horiz: ×
Tick interval = 10^{-6} KA m^{-1} Vert: ▲
DCZ016 Geographic AF Demag

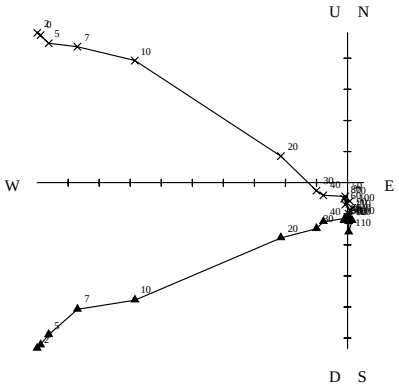

Horiz: ×
Tick interval = 10^{-6} KA m^{-1} Vert: ▲

DCZ017 Geographic AF Demag

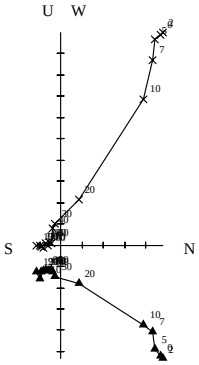

Horiz: ×
Tick interval = 10^{-6} KA m^{-1} Vert: ▲

DCZ017 Geographic AF Demag

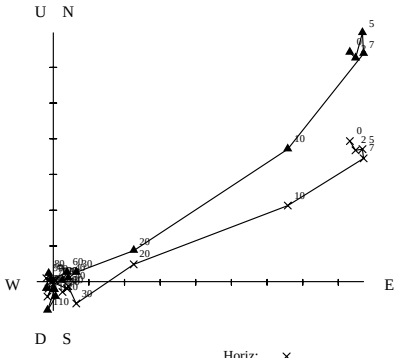

Horiz: ×
Tick interval = 10^{-6} KA m^{-1} Vert: ▲

DCZ018 Geographic AF Demag

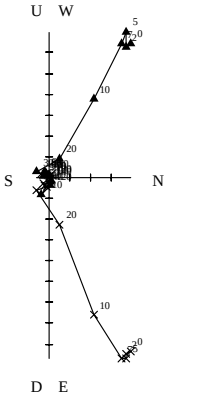

Horiz: ×
Tick interval = 10^{-6} KA m^{-1} Vert: ▲

DCZ018 Geographic AF Demag

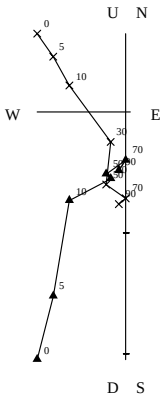

Horiz: ×
Tick interval = 10^{-6} KA m^{-1} Vert: ▲

DCZ019 Geographic AF Demag

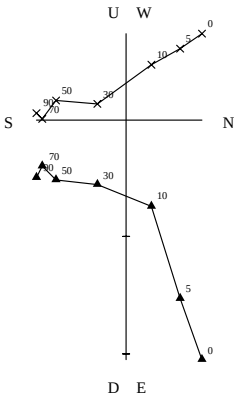

Horiz: ×
Tick interval = 10^{-6} KA m^{-1} Vert: ▲

DCZ019 Geographic AF Demag

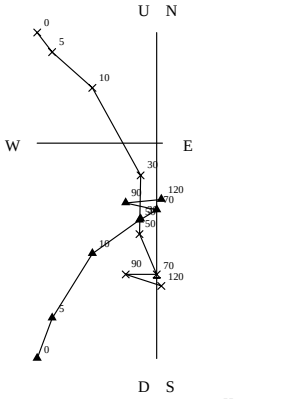

Horiz: ×
Tick interval = 10^{-6} KA m^{-1} Vert: ▲
DCZ020 Geographic AF Demag

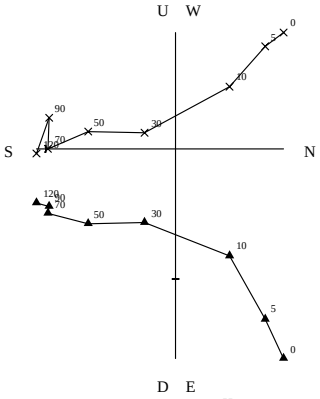

Horiz: ×
Tick interval = 10^{-6} KA m^{-1} Vert: ▲
DCZ020 Geographic AF Demag

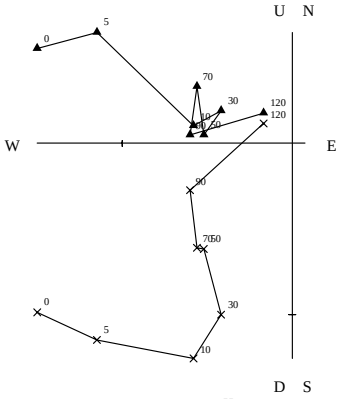

Horiz: ×
Tick interval = 10^{-6} KA m^{-1} Vert: ▲
DCZ021 Geographic AF Demag

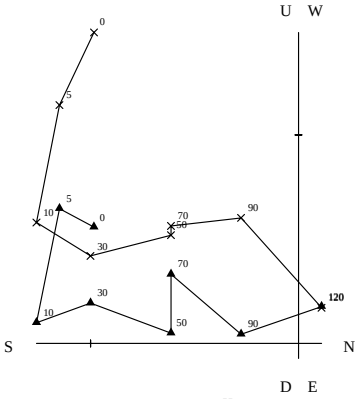

Horiz: ×
Tick interval = 10^{-6} KA m^{-1} Vert: ▲
DCZ021 Geographic AF Demag

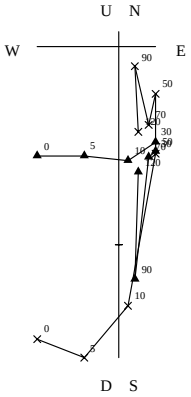

Horiz: ×
Tick interval = 10^{-6} KA m^{-1} Vert: ▲
DCZ022 Geographic AF Demag

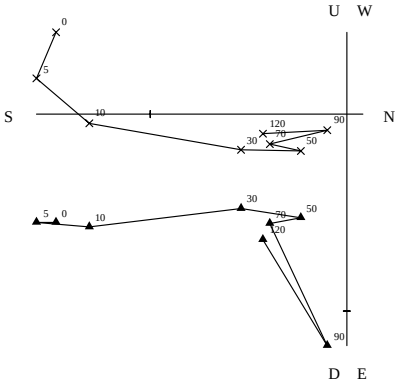

Horiz: ×
Tick interval = 10^{-6} KA m^{-1} Vert: ▲
DCZ022 Geographic AF Demag

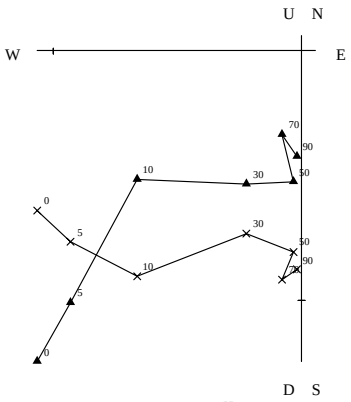

Horiz: ×
Tick interval = 10^{-6} KA m^{-1} Vert: ▲
DCZ023 Geographic AF Demag

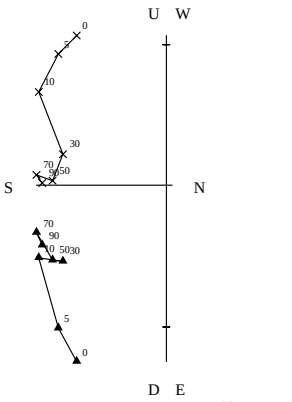

Horiz: ×
Tick interval = 10^{-6} KA m^{-1} Vert: ▲
DCZ023 Geographic AF Demag

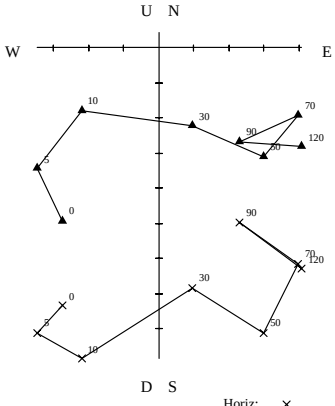

Horiz: ×
Tick interval = 10^{-7} KA m^{-1} Vert: ▲
DCZ024 Geographic AF Demag

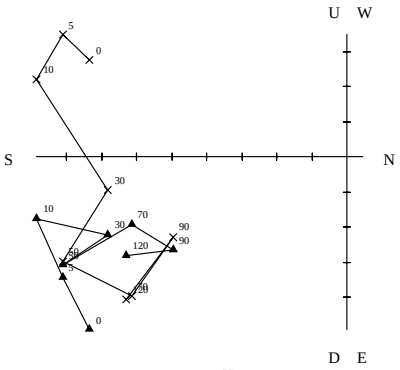

Horiz: ×
Tick interval = 10^{-7} KA m^{-1} Vert: ▲
DCZ024 Geographic AF Demag

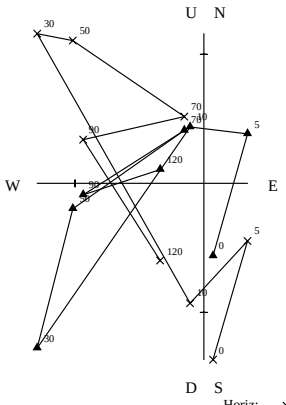

Horiz: ×
Tick interval = 10^{-7} KA m^{-1} Vert: ▲
DCZ025 Geographic AF Demag

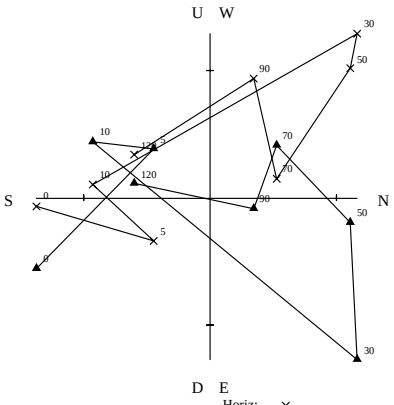

Horiz: ×
Tick interval = 10^{-7} KA m^{-1} Vert: ▲
DCZ025 Geographic AF Demag

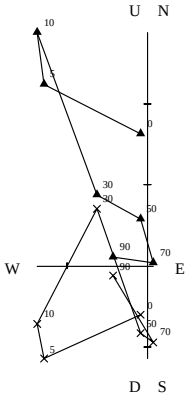

Horiz: ×
Tick interval = 10^{-7} KA m^{-1} Vert: ▲

DCZ026 Geographic AF Demag

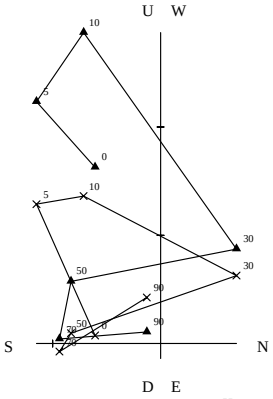

Horiz: ×
Tick interval = 10^{-7} KA m^{-1} Vert: ▲

DCZ026 Geographic AF Demag

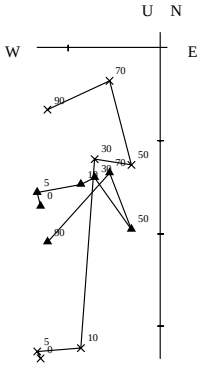

Horiz: ×
Tick interval = 10^{-7} KA m^{-1} Vert: ▲

DCZ027 Geographic AF Demag

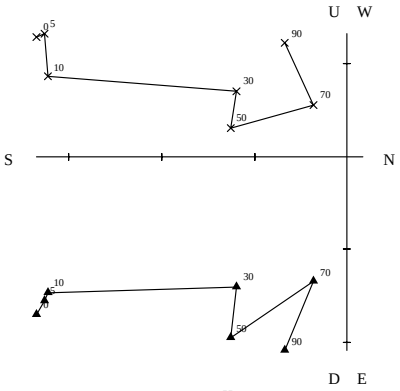

Horiz: ×
Tick interval = 10^{-7} KA m^{-1} Vert: ▲

DCZ027 Geographic AF Demag

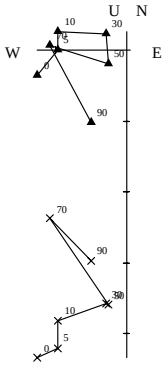

Horiz: ×
Tick interval = 10^{-7} KA m^{-1} Vert: ▲

DCZ028 Geographic AF Demag

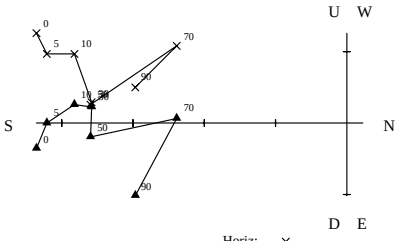

Horiz: ×
Tick interval = 10^{-7} KA m^{-1} Vert: ▲

DCZ028 Geographic AF Demag

APPENDIX E

MAGNETIC SUSCEPTIBILITY OF PALEOMAGNETIC SAMPLES

Sample	Number	**Mean** (cgs "volume")		**Standard Deviation**	
		Orientation 1	**Orientation 2**	**Orientation 1**	**Orientation 2**
DCZ	1	2.06E-05	2.22E-05	1.43E-06	1.42E-07
DCZ	2	2.76E-05	2.52E-05	2.21E-06	7.13E-07
DCZ	3	2.00E-05	1.86E-05	9.27E-07	1.78E-07
DCZ	4	2.00E-05	1.83E-05	3.57E-07	0.00E+00
DCZ	5	3.55E-05	1.40E-05	9.20E-05	6.42E-07
DCZ	6	1.97E-05	1.90E-05	1.14E-06	3.52E-08
DCZ	7	5.60E-06	7.70E-06	3.57E-08	3.57E-07
DCZ	8	7.74E-06	6.38E-06	6.77E-07	2.50E-07
DCZ	9	2.58E-05	2.55E-05	1.07E-07	2.85E-07
DCZ	10	2.98E-05	3.54E-05	3.92E-07	7.45E-06
DCZ	11	1.22E-05	1.23E-05	6.06E-07	1.43E-07
DCZ	12	1.19E-05	1.16E-05	3.29E-09	1.07E-07
DCZ	13	6.49E-06	5.03E-06	4.28E-07	5.35E-07
DCZ	14	6.77E-06	7.17E-06	7.13E-07	4.63E-07
DCZ	15	1.94E-05	1.83E-05	1.82E-06	5.70E-07
DCZ	16	3.23E-05	3.40E-05	3.57E-08	4.63E-07
DCZ	17	3.71E-05	3.67E-05	9.27E-07	2.50E-07
DCZ	18	5.89E-05	5.82E-05	2.50E-07	1.79E-07
DCZ	19	1.91E-05	1.83E-05	3.92E-07	1.78E-07
DCZ	20	1.85E-05	1.96E-05	6.06E-07	3.21E-07
DCZ	21	1.20E-05	1.30E-05	5.70E-07	9.27E-07
DCZ	22	1.22E-05	1.19E-05	6.77E-07	1.07E-07
DCZ	23	1.43E-05	1.33E-05	1.43E-07	3.47E-09
DCZ	24	9.02E-06	9.13E-06	3.58E-08	2.14E-07
DCZ	25	4.24E-06	3.78E-06	1.53E-06	1.07E-06
DCZ	26	5.24E-06	1.78E-06	2.03E-06	3.57E-07
DCZ	27	6.10E-06	6.06E-06	1.78E-07	6.42E-07
DCZ	28	6.92E-06	6.20E-06	4.28E-07	2.14E-07

APPENDIX F

PALEOFLOW MEASUREMENT AND CALCULATIONS

Explanation of Column Headings			
Location	Section (NE = Northern Extension, WS = Western Section, BBBB = Bob's Big Break Borehole, or SE = Southwest Extension)/Approximate location or survey station		
Quantity	Number of Paleo-indicators		
Scallop Length (cm)	Horizontal Measurement of Scallop in cm		
Direction Flow	Flow Direction indicated by Scallop		
Other misc.	Other Comments		
Cross Section of cave passage Area (modeled as an ellipse (m^2)	Product of vertical and horizontal passage dimensions divided by two then multiplied by pi	$A = \pi\left[\left(\frac{L+R}{2}\right)\times\left(\frac{U+D}{2}\right)\right]$ *L* = left, *R* = right, *U* = up, *D* = down (distance from survey station)	
Re (Reynolds Number)	Calculated by scallop length and ellipse diameter	$\mathrm{Re} = \mathrm{Re}^{\circ}\left[2.5\left(\ln\frac{D}{2L} - 1.5\right) + Bl\right]$ Re° = 2200, *D* = Diameter of passage, *L* = Scallop length, *Bl* = 9.4	
Average Velocity (cm/s)	Calculated by Re and scallop length	$\mathrm{Re} = \frac{V \times L \times \rho}{\eta}$ From Curl (1974)	$V = \mathrm{Re}\frac{\eta}{L \times \rho}$ Re-written for *V*
Discharge (m^3/s)	2/3 (Ellipse Area *Average Velocity) /1 million (use of 2/3 assumes passage is not full) (use of division by 1 million to convert cm^3 to m^3)	$Q = \left[\left(\frac{2}{3}A\right)xV\right] \div 1000000$	

Location	Quantity	Scallop Length (cm)	Direction Flow	Other misc.	Ellipse X-Section Area (m^2)	Re (Reynolds Number)	Average Velocity (cm/s)	Discharge (m^3/s)
SE/HAP 9	4	30.48	--	High on wall	58.71	27767.23	11.11	4.35
SE/TWA 15-16	2	20.12	E	--	3.65	23162.37	14.04	0.34
SE/TWA 14-16	2	15.24	E	on right wall	3.50	23462.05	18.77	0.44
SE/TWA 5	several	30.48	W	Just before survey station	2.35	22727.63	9.09	0.14
SE/TWA 6	3	30.48	S	On wall of SWE	2.92	24689.34	9.88	0.19
SE/HAP 20	2	35.36	N	On E Wall of SWE Just behind HAP 21	21.88	26103.09	9.00	1.31
SE/TWA 26	2	45.72	N	--	8.20	23686.57	6.32	0.35
SE/TWA 26	1	20.12	S	Also looks like a rock fell out of wall	8.20	28201.97	17.10	0.94
SE/HAP 27	3	60.96	N	On West Wall 6inches deep	30.34	23462.05	4.69	0.95
SE/HAP 30	1	91.44	N	on west Wall 6inches deep partially filled with formation	22.46	20497.57	2.73	0.41

Location	Quantity	Scallop Length (cm)	Direction Flow	Other misc.	Ellipse X-Section Area (m^2)	Re (Reynolds Number)	Average Velocity (cm/s)	Discharge (m^3/s)
SE/HAP 44	5	60.96	N	--	22.46	22727.63	4.55	0.68
SE/RRS 11	6	10.06	N	small	8.20	25392.43	30.79	1.68
SE/RRS 11	3	30.48	N		8.20	19294.78	7.72	0.42
SE/RRS 11	1	60.96	N	Large	8.20	15482.47	3.10	0.17
SE/RRS 11	1	30.48	S	--	8.20	19294.78	7.72	0.42
SE/PEF 19	2	20.12	N	--	23.63	26395.19	16.00	2.51
SE/TGS 22	1	30.48	S	West wall	36.10	29149.46	11.66	2.81
SE/TGS 22	2	30.48	N	West wall	36.10	29149.46	11.66	2.81
SE/TGS 22	1	30.48	N	West wall	36.10	29149.46	11.66	2.87
SE/HAQ 1	10	60.96	N	small conduit	0.98	6630.56	1.33	0.01

Location	Quantity	Scallop Length (cm)	Direction Flow	Other misc.	Ellipse X-Section Area (m^2)	Re (Reynolds Number)	Average Velocity (cm/s)	Discharge (m^3/s)
SE/HAQ 25	3	20.12	W	High on wall	1.53	16540.52	10.03	0.1
SE/HAQ 26	5	15.24	E	deep scallops	2.92	20877.03	16.71	0.33
SE/BKY 24	4	60.96	N	--	1.09	15482.47	3.10	0.02
SE/AFTER BKY 47	5	60.96	N	--	17.50	20877.03	4.18	0.49
SE/BKY 40	12	60.96	N	Many more	8.02	17064.72	3.41	0.18
SE/MOZ 20	6	30.48	N	Many more	7.58	22320.04	8.93	0.45
SE/HSB 1	3	30.48	W	--	21.08	23795.49	9.52	1.34
SE/MOZ 31	1	91.44	N	--	3.50	9795.07	1.31	0.03
SE/MOZ 31	1	30.48	S	--	3.50	15837.43	6.34	0.15
SE/HCB 7	3	30.48	W	On N wall	25.67	23462.05	9.39	1.61

Location	Quantity	Scallop Length (cm)	Direction Flow	Other misc.	Ellipse X-Section Area (m^2)	Re (Reynolds Number)	Average Velocity (cm/s)	Discharge (m^3/s)
SEHCB 7	1	45.72	W	--	25.67	21231.99	5.66	0.97
SE/SWE Express (beginning)	6	60.96	N	--	32.82	23107.09	4.62	1.01
NE/RB 29	1	121.92	N	--	33.18	20142.61	2.01	0.45
NE/RB 35	1	30.48	N	--	19.25	25692.11	10.28	1.32
NE/RB 35	1	30.48	S	--	19.25	25692.11	10.28	1.32
NE/RB35	1	60.96	S	--	19.25	21879.80	4.38	0.56
NE/RB 35	1	60.96	S	--	19.25	21879.80	4.38	0.56
NE/137	10	7.62	--	west wall	4.31	24200.36	38.73	1.10
NE/AU 32	5	15.24	NE	Perfect	10.43	25213.55	20.18	1.40
NE/AU 32	3	15.24	SW	--	10.43	25213.55	20.18	1.40

Location	Quantity	Scallop Length (cm)	Direction Flow	Other misc.	Ellipse X-Section Area (m^2)	Re (Reynolds Number)	Average Velocity (cm/s)	Discharge (m^3/s)
NE/AU 48	10	60.96	E	--	0.29	8212.81	1.64	0.003
NE/DD 25	2	91.44	N	--	17.94	15837.43	2.11	0.25
NE/DD 25	several	15.24	N	--	17.94	25692.11	20.56	2.46
NE/DD 25	band	15.24	N	all along wall	17.94	25692.11	20.56	2.46
NE/DD 11	1	22.86	N	--	6.42	21231.99	11.33	0.49
NE/DD 21	10	15.24	S	in dome after delightful dig	7.00	25692.11	20.56	0.96
NE/DD 92	3	10.06	S	poor quality	0.66	24165.14	29.30	0.13
NE/DD 102	1	30.48	N	--	2.92	15837.43	6.34	0.12
NE/DD 114	1	45.72	N	--	1.17	9795.07	2.61	0.02
NE/DD 104	3	45.72	N	--	7.66	14834.66	3.96	0.20

Location	Quantity	Scallop Length (cm)	Direction Flow	Other misc.	Ellipse X-Section Area (m^2)	Re (Reynolds Number)	Average Velocity (cm/s)	Discharge (m^3/s)
NE/DD 109	3	20.12	E	--	3.06	20352.83	12.34	0.25
NE/DD 57	3	30.48	S	very poor / lack of evidence	32.38	21879.80	8.75	1.89
NE/DD 19	3	25.39	S	--	1.02	16842.40	8.09	0.06
NE/DD 12	3	20.12	S	middle	9.92	21935.08	13.30	0.88
NE/AU 30	3	30.48	S	--	5.62	18915.32	7.57	0.28
NE/AU 15	3	20.12	S	--	3.28	25392.43	15.39	0.34
NE/AU 21	continuous layer	15.24	S	--	0.15	15837.43	12.67	0.01
NE/HE 10	20	76.20	S	big and perfect	6.13	16840.20	2.70	0.11
NE/AU 15	3	91.44	S	--	3.28	17064.72	2.28	0.05
NE/AU 15	8	10.06	N	--	3.28	29204.74	35.41	0.78

Location	Quantity	Scallop Length (cm)	Direction Flow	Other misc.	Ellipse X-Section Area (m^2)	Re (Reynolds Number)	Average Velocity (cm/s)	Discharge (m^3/s)
NE/AU 6	3	30.48	S	--	2.33	15837.43	6.34	0.10
NE/AU 2	30	15.24	W	--	51.05	31579.54	1.81	8.6
NE/HE 19	1	91.44	E	--	4.08	13607.38	3.01	0.5
NE Extension	complete bands	30.48	S	--	1.51	23511.966	9.04	0.09
EN/NF 10	7	30.48	S	--	32.23	22320.04	3.70	1.91
NE/NF 10	7	60.96	S	no question along walls direction of paleoflow	32.23	18507.73	2.28	0.80
WS/Dune Room	2	15.24	NE	--	57.76	31316.93	25.06	9.56
WS/Dune Room	2	121.92	SE	1ft. Deep	57.76	19880.00	1.99	0.76
WS/Forrest Room	1	15.24	W	poor	12.33	28012.67	22.42	1.82
WS/AG 18	2	15.24	N	--	1.75	21281.91	17.03	0.20

Location	Quantity	Scallop Length (cm)	Direction Flow	Other misc.	Ellipse X-Section Area (m^2)	Re (Reynolds Number)	Average Velocity (cm/s)	Discharge (m^3/s)
Flowstone River Passage	4	30.48	W	--	4.08	20702.43	8.28	0.22
No Name Room	6	22.86	W	--	26.20	26537.22	14.16	2.45